Title

Epithelial-to-mesenchymal transition supports ovarian carcinosarcoma tumorigenesis and confers sensitivity to microtubule-targeting with eribulin

Authors and Affiliations

Gwo Yaw Ho[1,2,3^], Elizabeth L. Kyran[1,2,4^], Justin Bedo[1,5^], Matthew J. Wakefield[1,6^], Darren P. Ennis[7,8], Hasan B. Mirza[7], Cassandra J. Vandenberg[1,2], Elizabeth Lieschke[1,2], Andrew Farrell[1], Anthony Hadla[1,2], Ratana Lim[1], Genevieve Dall[1,2], James E. Vince[1,2], Ngee Kiat Chua[1], Olga Kondrashova[1], Rosanna Upstill-Goddard[8], Ulla-Maja Bailey[8], Suzanne Dowson[8], Patricia Roxburgh[8,9], Rosalind M. Glasspool[8,9], Gareth Bryson[10]; Andrew V. Biankin[8]; for the Scottish Genomes Partnership, Susanna L. Cooke[8], Gayanie Ratnayake[3], Orla McNally[3,6,12]; Nadia Traficante[11,12]; for the Australian Ovarian Cancer Study[11,13]**,** Anna DeFazio[13,14,15], S. John Weroha[16], David D. Bowtell[11,12], Iain A. McNeish[7,8,9#], Anthony T. Papenfuss[1,2,11#], Clare L. Scott[1,2,3,6,12#], Holly E. Barker[1,2#*]

[1]The Walter and Eliza Hall Institute of Medical Research, Parkville, Victoria, 3052, Australia.
[2]Department of Medical Biology, University of Melbourne, Parkville, Victoria, 3010, Australia.
[3]The Royal Women's Hospital, Parkville, Victoria, 3052, Australia.
[4]Cancer Research UK Cambridge Institute, Cambridge CB2 0RE, UK.
[5]School of Computing and Information Systems, the University of Melbourne, Parkville, Victoria, 3010, Australia.
[6]Department of Obstetrics and Gynaecology, University of Melbourne, Parkville, Victoria 3010, Australia.
[7]Division of Cancer and Ovarian Cancer Action Research Centre, Department of Surgery and Cancer, Imperial College London, London W12 0NN, UK.
[8]Institute of Cancer Sciences, Wolfson Wohl Cancer Research Centre, University of Glasgow, Glasgow G61 1QH, UK.
[9]Beatson West of Scotland Cancer Centre, Glasgow G12 0YN, UK.
[10]Department of Pathology, Queen Elizabeth University Hospital, Glasgow G51 4TF, UK.
[11]Research Division, Peter MacCallum Cancer Centre, 305 Grattan Street, Melbourne, Victoria, 3000, Australia.
[12]Sir Peter MacCallum Cancer Centre Department of Oncology, University of Melbourne, Parkville, Victoria, 3010, Australia.

[13]Centre for Cancer Research, The Westmead Institute for Medical Research, Sydney, NSW 2145, Australia.
[14]The Daffodil Centre, The University of Sydney, a joint venture with Cancer Council NSW, Sydney, NSW 2145, Australia.
[15]Department of Gynaecological Oncology, Westmead Hospital, Sydney, NSW, 2145, Australia.
[16]Department of Oncology, Mayo Clinic, Rochester, Minnesota, US.

^ authors contributed equally to work
# Senior authors; contributed equally to work
* Correspondence: barker.h@wehi.edu.au

Running title

Ovarian carcinosarcoma genomics and eribulin response

Keywords

Ovarian carcinosarcoma, epithelial-to-mesenchymal transition (EMT), eribulin, N-MYC, mevalonate pathway

Corresponding author

Dr Holly Barker
Cancer Biology and Stem Cells Division
The Walter and Eliza Hall Institute of Cancer Research
1G Royal Pde,
Parkville,
Victoria, 3052,
Australia
Ph: +61 414 419 741
Fax: +61 3 9345 0852
Email: barker.h@wehi.edu.au

Conflict of interest disclosure statement

Eisai Inc provided drug support for this study. R.M.G. declares Advisory boards for Clovis, Tesaro and AstraZeneca. A.V.B. declares Personal and Financial interest in BMS, AstraZeneca, MyTomorrows, Elstar Therapuetics, IP Financial Interest in Agilent Technologies, Leadership role, stock ownership in Cumulus Oncology, Nodus Oncology, ConcR, Cambridge Cancer Genomics. IAMcN declares Advisory Boards for Clovis Oncology, Tesaro/GSK, AstraZeneca, Roche, Scancell, Carrick Therapeutics, Takeda Oncology; Institutional grant support from AstraZeneca. ADeF declares Research Support from AstraZeneca. D.D.B. declares Consultant for Exo Therapeutics. Research Support for AstraZeneca, Roche, GNE, Beigene. C.L.S. declares Advisory Boards for AstraZeneca, Clovis Oncology, Roche, Eisai Inc, Sierra Oncology, Takeda, MSD and Grant/Research support from Clovis Oncology, Eisai Inc, Sierra Oncology, Roche and Beigene. Other authors declare no conflicts of interest.

Word count: 5159 (not including abstract, significance, materials and methods or references)
Display items: 6 Figures, 2 Tables
References: 56

Abstract

Ovarian carcinosarcoma (OCS) is an aggressive and rare tumour type with limited treatment options. OCS is hypothesised to develop via the combination theory, with a single progenitor resulting in carcinomatous and sarcomatous components, or alternatively via the conversion theory, with the sarcomatous component developing from the carcinomatous component through epithelial-to-mesenchymal transition (EMT). In this study, we analysed DNA variants from isolated carcinoma and sarcoma components to show that OCS from 18 women is monoclonal. RNA sequencing indicated the carcinoma components were more mesenchymal when compared with pure epithelial ovarian carcinomas, supporting the conversion theory and suggesting that EMT is important in the formation of these tumours. Preclinical OCS models were used to test the efficacy of microtubule-targeting drugs, including eribulin, which has previously been shown to reverse EMT characteristics in breast cancers and induce differentiation in sarcomas. Vinorelbine and eribulin more effectively inhibited OCS growth than standard-of-care platinum-based chemotherapy, and treatment with eribulin reduced mesenchymal characteristics and N-MYC expression in OCS patient-derived xenografts (PDX). Eribulin treatment resulted in an accumulation of intracellular cholesterol in OCS cells, which triggered a down-regulation of the mevalonate pathway and prevented further

cholesterol biosynthesis. Finally, eribulin increased expression of genes related to immune activation and increased the intratumoral accumulation of CD8+ T cells, supporting exploration of immunotherapy combinations in the clinic. Together, these data indicate EMT plays a key role in OCS tumorigenesis and support the conversion theory for OCS histogenesis. Targeting EMT using eribulin could help improve OCS patient outcomes.

Significance

Genomic analyses and preclinical models of ovarian carcinosarcoma support the conversion theory for disease development and indicate that microtubule inhibitors could be used to suppress EMT and stimulate anti-tumour immunity.

Introduction

Ovarian carcinosarcoma (OCS), also known as malignant mixed Müllerian tumour, is a heterogeneous cancer with poor prognosis (1), accounting for 1-4% of ovarian malignancies (2,3). These tumours contain both epithelial (carcinoma) and mesenchymal (sarcoma) components (3). Molecular analysis suggests that most OCS are monoclonal (4-9), with two theories for OCS histogenesis: combination, where a single stem cell differentiates early to form the two components; and conversion, where the carcinoma undergoes epithelial-to-mesenchymal transition (EMT) to form the sarcomatous component (10).

TP53 mutations and loss of heterozygosity (LOH) of 17p, and consequent chromosomal instability, are common in OCS (7,8,11,12). Mutations in *PIK3CA*, *PTEN*, *KRAS*, *FBXW7*, *CTNNB1*, and *RB1* are observed frequently (11), whilst mutations in *ARID1A*, *ARID1B*, *KMT2D*, *BAZ1A*, *BRCA1*, *BRCA2*, and *RAD51C* have also been reported (8,11,13). One study also identified recurrent mutations in the genes encoding histones H2A and H2B (*HIST1H2AB*/*C*, *HIST1H2BB*/*G*/*J*) that play a role in EMT (9). Only one study has analysed gene expression in the separate components, finding a strong positive correlation of EMT score with sarcoma content as well as methylation of the EMT-suppressing miRNAs miR-141/200a/200b/200c/429 (8).

EMT can be induced through aberrant expression of the high-mobility-group AT-hook protein 2 (HMGA2) and subsequent activation of the TGFβ signalling pathway (14). HMGA2 is not expressed in most adult tissues (15,16), but high expression has been observed in many cancers and is correlated with metastasis and chemotherapy resistance (17-21). HMGA2 expression is

thought to be largely controlled by the microRNA *let-7* (22). Other downstream target genes of *let-7* include *MYCN* and *LIN28B*, whilst LIN28B inhibits maturation of *let-7* (23), reinforcing both low and high expression states and acting as a bistable switch. Up-regulation of the N-MYC/LIN28B pathway has been observed in the C5 subset of ovarian or fallopian tube high-grade serous carcinoma (HGSC) and in other cancer subtypes, and is associated with poor prognosis (23-25). Furthermore, high HMGA2 expression has been observed in 60% of OCS cases (26). We hypothesised that up-regulation of the N-MYC/LIN28B pathway and subsequent expression of HMGA2 may be a key driver of OCS, and thus drugs that target EMT may be effective.

Eribulin is a microtubule-targeting drug that has been shown to reverse EMT, leading to favourable intra-tumoural vascular remodelling, reduced cell invasion, increased cell differentiation, and modulation of the tumour-immune microenvironment (27-29). Eribulin has completed Phase III trials for metastatic breast cancer, soft-tissue sarcoma and non-small cell lung cancer (NSCLC) (30-33). Eribulin was initially approved by the US Food and Drug Administration (FDA) and the European Medicines Agency (EMA) in 2010 and 2011, respectively, for treatment of advanced breast cancer, with later approvals for advanced liposarcoma (28,33). We hypothesised that eribulin may be effective against OCS tumours due to its ability to reverse EMT characteristics, alter tumour phenotype and affect the tumour microenvironment through effects on the vasculature.

Here we present mutation, copy number and gene expression analyses of separate components from an OCS cohort. We have used a highly relevant genetically engineered mouse model (GEMM), which replicates features of the human condition, as well as patient-derived xenograft (PDX) models of OCS to assess the efficacy of a range of microtubule-targeting drugs and to determine the mechanism of action of eribulin, a drug with significant activity in these models.

Materials and Methods:

Study conduct, survival analyses and patient samples

Samples for the UK cohort were acquired and utilised under the authority of the NHS Greater Glasgow and Clyde Biorepository (Application Reference 286) following approval by West of Scotland Research Ethics Committee 4 (Reference 10/S0704/60). Overall survival was calculated from the date of diagnosis to the date of death or the last known clinical assessment.

Overall survival was calculated by log-rank test (Mantel-Cox) using Prism v8.0 (GraphPad, San Diego, CA).

Formalin-fixed paraffin-embedded (FFPE) specimens were identified from the pathology archives of Queen Elizabeth University Hospital, Glasgow, UK. Carcinoma and sarcoma regions were identified and marked by a gynaecological pathologist.

Panel Sequencing

Libraries for panel sequencing of isolated carcinoma and sarcoma regions of patient tumours were prepared from genomic DNA (gDNA) obtained from 5 x 10µm macro-dissected FFPE sections. Panel sequencing enabled analysis of 217 genes for coding sequence mutations, 137 genes for copy number state, and 23 genes for all genomic events. In addition, SNPs spaced approximately 1Mb apart throughout the genome were included to give a genome-wide copy number profile. Full details of library preparation, panel design and sequencing analysis are provided in Supplementary Materials and Methods.

RNA preparation and sequencing

Libraries for RNA sequencing (RNAseq) of isolated carcinoma and sarcoma regions of patient tumours were prepared from RNA obtained from 5 x 10µm macro-dissected FFPE sections. Libraries underwent 75bp paired-end sequencing on a HiSeq 4000 sequencer (Illumina). The HGSC samples from TCGA (TCGA-OV cohort) (n=396) used for comparison were obtained from RNAseq_V2 processed counts downloaded from the GDC portal (https://portal.gdc.cancer.gov/), version available on 3rd June 2019.

Libraries for RNAseq of PDX tumours were prepared from RNA extracted using the Direct-zol™ RNA Miniprep kit (Zymo Research) as per manufacturer's instructions. Sequencing was performed on the Novaseq platform (Illumina) to read length of 100 bp (Australian Genome Research Facility). All analysis was performed on human specific reads, purified by competitive mapping of the reads to both the human and mouse genomes using our published opensource Xenomapper method (34). DEGs between treated and untreated samples were derived using matching methods across batch and model to correct for batch effects and inherent model differences. *p*-values for DEGs were computed under a normality assumption. Topconfects (35) was used to calculate lower bounds on the effect sizes with 95% confidence.

Full details of RNAseq library preparation and sequencing analysis are provided in Supplementary Materials and Methods.

Generation of a genetically-engineered mouse model (GEMM)

The *Pax8-rtTA* strain (C57BL/6 background) was a kind gift from Prof Ronny Drapkin (University of Pennsylvania, Department of Obstetrics and Gynecology, US). The *kai-tetOCre* strain (FVB background) was a kind gift from Prof Jane Visvader (WEHI, Melbourne, Australia) originally sourced from the Osaka Bioscience Institute, Japan. The *LSL-Lin28b* strain (mixed 129X1/SvJ background) was a kind gift from Prof Johannes H. Schulte (University Hospital Essen, Germany). Full details about GEMM OCS tumour generation are available in Supplementary Materials and Methods.

Immunohistochemistry

Formalin fixed tumour samples were sectioned, stained with haematoxylin and eosin (H&E), or the following antibodies: anti-Ki67 (mouse: D3B5, Cell Signalling; human: MIB-1, Dako), anti-PAX8 (Proteintech Cat# 10336-1-AP, RRID:AB_2236705), anti-p53 (mouse: CM5, Novacastra; human: DO-7, Dako), anti-PanCK (mouse: polyclonal, Abcam; human: AE1/3, Dako), anti-vimentin (Cell Signaling Technology Cat# 5741, RRID:AB_10695459), anti-HMGA2 (Cell Signaling Technology Cat# 8179, RRID:AB_11178942), anti-N-cadherin (Abcam Cat# ab18203, RRID:AB_444317), anti-ZEB1 (Novus Cat# NBP1-05987, RRID:AB_2273178), anti-human CD8 (C8/144B, Dako). H&E and IHC slides were scanned digitally at 20x magnification using the Pannoramic 1000 scanner (3DHISTECH Ltd.). Ki67 and CD8 IHC was quantified using CellProfiler™ (Broad Institute).

Western Blot Analysis

Tumours and cells were homogenised in ice-cold RIPA buffer supplemented with a complete mini protease inhibitor cocktail tablet (Roche) using Precellys Ceramic Kit tubes in the Precellys 24 homogenising instrument (Thermo Fisher Scientific). Proteins from lysates were separated on NuPAGE® Novex® Bis-Tris 10% gels (Invitrogen). Gels were transferred onto PVDF membranes using the iBlot™ Transfer system (Thermo Fish Scientific). Membranes were probed with antibodies specific for ZEB1, N-cadherin, vimentin, HMGA2 (all as mentioned previously), N-MYC (Cell Signaling Technology Cat# 84406, RRID:AB_2800038)), HMGCS (A-6, Santa Cruz), SQLE, LDLR (Proteintech Cat# 12544-1-

AP, RRID:AB_2195888 and Proteintech Cat# 10785-1-AP, RRID:AB_2281164), Cleaved-Caspase 3 and cleaved-PARP-1 (Cell Signaling Technology Cat# 9661, RRID:AB_2341188 and Cell Signaling Technology Cat# 5625, RRID:AB_10699459), or β-actin (Sigma-Aldrich Cat# A5441, RRID:AB_476744).

***In vivo* studies**

All experiments involving animals were performed according to the animal ethics guidelines and were approved by the Walter and Eliza Hall Institute (WEHI) of Medical Research Animal Ethics Committee (2016.023). PDX #1040 was generated from ascites obtained from a patient treated at the Royal Women's Hospital, Melbourne, and recruited to the Australian Ovarian Cancer Study. The PDX was established by mixing tumour cells isolated from ascites with Matrigel Matrix (Corning) and transplanting subcutaneously into NOD/SCID/IL2Rγnull recipient mice (T1=passage 1). PDX #1105 and #1177 were established through transplanting fragments of tumour tissue obtained from patients consented to the Stafford Fox Rare Cancer Program (WEHI, Melbourne, Australia). All other PDXs were established through transplanting fragments of cryopreserved tumour tissue subcutaneously from PDXs generated in the Mayo Clinic (USA). Recipient mice bearing T2-T7 PDX or GEMM tumours (180-300 mm^3 in size) were randomly assigned to cisplatin (Pfizer), pegylated liposomal doxorubicin (PLD; Janssen-Cilag Pty. Ltd.), paclitaxel (Bristol-Myers Squibb), vinorelbine (Pfizer), eribulin (Eisai Co., Ltd.), or vehicle treatment groups. *In vivo* cisplatin treatments were performed by intraperitoneal (IP) injection of 4 mg/kg given on days 1, 8 and 18. The regimen for PLD treatment was by IP injection once a week for three weeks at 1.5 mg/kg. The regimen for paclitaxel treatment was by IP injection twice a week for three weeks at 25 mg/kg. The regimen for vinorelbine was by intravenous injection of 15 mg/kg at days 1, 8 and 18. The regimen for eribulin treatment was by IP injection three times a week for three weeks at 1.5 mg/kg (with the exception of mice harbouring #1040 tumours, which received doses of 1 mg/kg with the same scheduling). Vehicle for cisplatin, PLD, paclitaxel, vinorelbine and eribulin treatment was Dulbecco's Phosphate Buffered Saline (DPBS). Harvested tumours were histologically assessed by a gynaecological pathologist, using sections stained with H&E, pan-cytokeratin and vimentin, to ensure both carcinoma and sarcoma components were present. See Supplementary Materials and Methods for dosing schedules and classification of treatment response. Data collection was conducted using the Studylog LIMS software (Studylog

Systems, San Francisco). Graphing and statistical analysis was conducted using the SurvivalVolume package (36).

A human immune system (HIS) was generated in NSG mice by reconstituting myeloablated newborn NSG pups with human CD34+ haematopoietic stem cells isolated from cord blood (purchased from Lonza, cat #2C-101). Briefly, two-day old pups were treated with 150 rads gamma-irradiation and following 2-3 hrs of recovery were injected via the facial vein with $5x10^4$ human CD34+ cells in 30-40 µL DPBS/0.02% trypan blue using a Hamilton syringe. Twelve-weeks post-reconstitution peripheral blood was obtained by retro-orbital bleed and analysed using an Advia 2120i and, following red cell depletion, by flow cytometry (mCD45-APC/Cy7 clone 30-F11, hCD45-APC clone HI30, hCD4-BV605 clone RPA-T4, hCD8-FITC clone RPA-T8, hCD3-PE/Cy7 clone UCHT1, and hCD19-PE HIB19; BD Biosciences). Mice with >25% hCD45 white blood cells were considered successfully engrafted HIS mice. Tumour fragments for OCS PDX #1105 and #1177 were transplanted subcutaneously into HIS mice. Once tumours reached $400mm^3$, mice were treated with a single dose of vehicle (DPBS) or eribulin (3mg/kg) and tumours were harvested one week later.

Generation of cell lines

The OCS GEMM cell line was generated from a T1 OCS GEMM tumour, the PH419 cell line was generated from a T3 PDX tumour, and the PH142 cell line was generated from a T5 PDX tumour. Briefly, tumours were manually minced into a slurry. For the GEMM cell line, cell fragments were subsequently plated on 0.1% gelatin coated plate and passaged aggressively within 3-4 days to retain viable malignant adherent cells until a stable cell line was obtained at passage 12 onward. For the PH419 and PH142 cell lines, the mince was digested with collagenase, dispase, and DNase (Worthington), with cells cultured in growth media for 10 passages. Cell identity was confirmed by genotyping (GEMM cell line) or TP53 sequencing (PH419 and PH142 cell lines). Short tandem repeat (STR) profiling has also been used to characterise these new OCS cell lines.

Adhesion, invasion assays and 3D growth assays

Adhesion assays were carried out in 96-well plates pre-coated with 2% BSA or 20 µg/ml collagen. GEMM cells were pre-treated for a week with DMSO (vehicle control), 0.2 µM cisplatin or 20 nM eribulin (IC_{20} concentrations for these drugs in these cells) before plating in

96-well plates. Non-adherent cells were aspirated and adherent cells stained with 100 µl of 0.5% crystal violet (Sigma) dissolved in 20% methanol for 15 minutes at room temperature. Stained cells were solubilised with 50 µl of 0.1 M citrate buffer in 50% methanol. Adherent cells were quantified by measuring absorbance at 595 nm on a Chameleon Luminescence Plate Reader (Noki Technologies). Transwell migration, invasion and 3D assays were carried out as previously described (37).

Quantification of cholesterol

Snap frozen cell pellets or tumour pieces were lysed in 1X reaction buffer on ice. Cholesterol was quantified using the Amplex Red Cholesterol Assay Kit (Invitrogen) as per manufacturer's instructions. Total cholesterol levels were quantified using buffer containing cholesterol esterase. Free cholesterol levels were quantified using buffer without cholesterol esterase. Cholesterol ester levels were calculated by subtracting the value of free cholesterol from total cholesterol.

Oil Red O staining

Snap frozen tumour pieces were set in Optimal Cutting Temperature (OCT) compound on dry ice and sectioned onto charged slides. Slides were incubated in Oil Red O solution, washed and counterstained with haematoxylin. Slides were scanned digitally at 20x magnification using the Pannoramic 1000 scanner (3DHISTECH Ltd.). Oil Red O staining was quantified using CellProfiler™ (Broad Institute).

Statistical Analysis

Data were analysed using the Student t-test unless otherwise stated and considered significant when the *p* value was <0.05. All statistical tests were two-sided. Bar graphs represent the mean and standard error across independent experimental repeats (at least n=3) unless otherwise stated. All boxplots demarkate the inter-quartile range (IQR) as the outer box and median as the contained break. Whiskers extend to the furthest point not exceeding 1.5 x IQR. Survival analysis was performed using the log rank test on Kaplan-Meier survival function estimates. Statistical significance representations: **p*<0.05, ***p*<0.01, ****p*<0.001, ****p*<0.0001.

Data availability

The following data sets have been deposited in the European Genome-Phenome Archive (EGA) under accession number EGAS00001006555: RNAseq data of the PDX samples, and TSO500 panel data, whole exome sequencing data, or whole genome sequencing data of the patient samples: PH003, PH006, PH142, PH419, PH592, #1105 and #1177. A data transfer agreement is required. The following data sets have been deposited in the EGA under accession number EGAS00001006605: DNA and RNA sequencing of patient samples in the UK cohort (n=18).

Results

Mutation and copy number profile of OCS is similar to HGSC

We identified 18 women diagnosed with OCS, 17 with high-grade serous carcinoma (HGSC) and one with grade 2 endometrioid histology in the carcinoma component. 12 associated metastatic samples were also available (Supplementary Table S1 and Supplementary Figure S1). As has previously been observed in uterine carcinosarcoma (38), the metastases in our cohort were more commonly purely carcinoma (8 carcinoma vs 4 sarcoma; Figure 1a and Supplementary Table S1). Targeted sequencing of 377 genes in macro-dissected carcinoma and sarcoma components as well as metastases was performed (Supplementary Tables S2-S7; Supplementary Figure S2).

Overall, OCS samples had genomic profiles similar to HGSC, with near-ubiquitous *TP53* mutation (17/18 cases, including 17/17 with HGSC pathology), *CCNE1* amplification (4/18 cases), *BRCA2* loss or mutation (4/18 cases), *KRAS* mutation and amplification (4/18 cases), *PIK3CA* mutation and amplification (4/18 cases), *NF1* or *CDKN2A* mutation or disruption by rearrangement (2/18 cases each), *RB1* deletion (2/18 cases), *PTEN* mutation (2/18 cases) and *MYC* or *MYCN* amplification (1/18 and 2/18 cases, respectively) (Figure 1a). Overall mutational burden was low (mean 1.2, median 0.87 mutations/MB sequenced), which did not differ between carcinoma and sarcoma (Figure 1b, Supplementary Table S8). However, as with HGSC, the genomes were structurally unstable with an average of 3.3 high-level gains and 1.4 likely homozygous deletions called per sample (Supplementary Figure S3). WW00163 lacked the genomic chaos typical of HGSC (Supplementary Figure S4), in keeping with an origin of endometrioid carcinoma.

Based on point mutation profiles, there were no consistent differences between the sarcoma and carcinoma components. In all cases, the two components shared at least one point mutation, demonstrating a shared clonal origin. Half of carcinoma-sarcoma pairs (8/16) shared all point mutations while the others gained additional mutation(s) in one or both components. On average, carcinoma-sarcoma pairs differed by only a single mutation (range 0-7). These data indicated that these 18 OCS were monoclonal, which supports both the conversion and combination theories of carcinogenesis.

By contrast, there were more copy number changes between the carcinoma and sarcoma components, with an average of 10.6 genes having a different copy number state between the two (range 0-36) (Supplementary Figures S3 and S4; Supplementary Table S6). The most commonly different genes were *FGF3* and *MDM2* (Supplementary Table S7). However, these differences did not appear to be focal or high level, perhaps suggesting that these genes are not specific targets of alteration between carcinomas and sarcomas. Instead these chromosomal differences may arise due to ongoing chromosomal instability. Case WW00169 had neither mutation nor copy number differences between the carcinoma and sarcoma components.

Interestingly, in some cases metastases showed substantial genomic divergence from their corresponding primary, indicative of an early seeding to the metastatic sites (Figure 1a). There was evidence of the metastases arising from the carcinomatous component (WW00158 and WW00170) as well as the sarcomatous component (WW00157). In addition to two cases (WW00154, WW00158) where the metastasis either gained three mutations or lost four, a third case (WW00157) diverged in several likely driver copy number events including loss of *BRCA2* between the carcinoma and its corresponding metastasis (Supplementary Tables S4, S6 and S7).

OCS have EMT-like and N-MYC pathway gene expression patterns

We next undertook RNAseq on isolated carcinoma (n=13) and sarcoma (n=9, 7 paired with carcinoma) components (Supplementary Figure S5; Supplementary Tables S9-S12). Using an EMT expression signature derived from uterine carcinosarcoma (39), we found a highly significant enrichment of EMT in carcinosarcomas, compared with the TCGA cohort of ovarian HGSC (TCGA-OV; n=379). This enrichment was predominantly driven by the sarcoma component, with the EMT score being significantly higher in the sarcoma component compared to the carcinoma component (p = 0.005; Figure 1c), and was confirmed using other

reported EMT signatures (Supplementary Figure S6a-e). However, the carcinoma components also had significantly higher EMT scores than the TCGA-OV cohort, suggesting that the OCS carcinoma component was either predisposed to undergo sarcomatous transformation or already transitioning to sarcoma ($p < 0.0001$; Figure 1c).

To study the N-MYC/LIN28B pathway specifically, we analysed *MYCN*, *LIN28B* and *HMGA2* expression in the same dataset. *LIN28B* and *HMGA2* were significantly up-regulated in carcinosarcomas compared to the TCGA-OV cohort ($p < 0.0001$ for both; Figure 1d). As expected from the high EMT scores observed in the carcinomatous components, expression of *LIN28B* and *HMGA2* were equally high in both components (Supplementary Figure S6f).

p53 inhibition and up-regulation of the N-MYC/LIN28B pathway in fallopian tube secretory epithelial cells gives rise to OCS

We established an OCS GEMM by directing both p53 inhibition and N-MYC/LIN28B pathway up-regulation to the fallopian tube secretory epithelial cell (FTSEC) via the PAX8 promoter (Supplementary Figure S7a). We included CRISPR-mediated knock-out of *Pten* in subsequent lines, also giving rise to OCS (Supplementary Table S13). The initial founder tumour (T0) from a *Pax8-rtTA;TetO-Cre;LSL-Lin28b;SV40Tag* mouse, first passage tumours (T1), and a stable cell line derived from a T1 tumour (OCS GEMM cells) were validated by genotyping (Supplementary Tables S14 and S15).

Tumours expressed high levels of p53, as well as cytokeratin (pan-CK) in approximately 5% and vimentin in approximately 95% of the regions analysed, indicating a predominantly sarcomatous phenotype (Supplementary Figure S7b). Quantitative RT-PCR confirmed elevated expression of *Lin28b* in both the tumour and cell line (Supplementary Figure S7c) and RNAseq confirmed up-regulation of *Lin28b* and *Mycn* in the tumours and up-regulation of *Lin28b* and *Hmga2* in the cell line, relative to control fallopian tubes (Supplementary Figure S7d; Supplementary Table S16).

GEMM tumours are resistant to current standard-of-care treatments but respond to the microtubule inhibitors vinorelbine and eribulin

We assessed the *in vivo* response of GEMM tumours to standard-of-care HGSC therapies, cisplatin, pegylated liposomal doxorubicin (PLD) and paclitaxel. Overall, the tumours were refractory to all three treatments, as the time to progressive disease (PD) was the same as for

vehicle treatment. PLD and cisplatin failed to demonstrate any meaningful response (Figure 2a), although paclitaxel demonstrated modest responses with an increase in median time-to-harvest (TTH) from 15 to 36 days compared to vehicle treatment (Table 1, p=0.0101, respectively). By contrast, significant tumour regression was observed in all tumours treated with the microtubule inhibitor vinorelbine leading to improvement of median TTH (15 days (vehicle) vs 81 days; Figure 2a, Table 1; p<0.0001). Eribulin also resulted in significant tumour regression in all tumours leading to improvement of median TTH (15 days vs 46 days; Figure 2a, Table 1; p<0.0001). Expression of Ki67 in the tumours was significantly reduced one week after mice received a single dose of eribulin (Figure 2b, p<0.001).

Eribulin treatment reduces adhesion, invasion and branching of the OCS GEMM cell line

In vitro functional assays showed eribulin reduced both adhesion to collagen matrices (Figure 2c; p=0.024) and invasion through extracellular matrices of OCS GEMM cells (Figure 2c; p=0.0042), compared to DMSO, and reduced branch formation in 3D collagen growth assays (Figure 2d). Western Blot analysis determined a reduction in expression of the mesenchymal markers ZEB1, N-cadherin, vimentin and HMGA2 in OCS GEMM cells exposed to eribulin (Figure 2e).

A cohort of OCS PDX models with N-MYC/LIN28B pathway up-regulation recapitulates the biphasic and heterogeneous nature of OCS

We next expanded and characterised six PDX models of OCS with varying proportions of carcinoma and sarcoma, all harbouring a mutation in *TP53* and other molecular features common to OCS (Figure 3a; Supplementary Tables S17 and S18). Pan-cytokeratin and vimentin expression indicated the carcinomatous and sarcomatous components, respectively. Two models, PH142 and PH006, contained cells co-expressing pan-cytokeratin and vimentin, which were confirmed by a gynaecological pathologist to have a mixed phenotype (Figure 3a). The heterogeneous characteristics of the PDX cohort resembled the human OCS tumour landscape. Furthermore, all PDX models expressed HMGA2, suggesting the N-MYC/LIN28B pathway was up-regulated. Over time, a purely sarcomatous lineage (PH003sarc) arose from the original mixed PH003 model (called PH003mixed). RNAseq data revealed that all PDX had higher HMGA2 expression and EMT scores than the epithelial ovarian cancer cohort TCGA-OV (Figures 3b and 3c). The most sarcomatous PDX models (PH003sarc and PH592) had higher EMT scores than models containing regions of pure carcinoma (PH419 and

PH003mixed). Interestingly, while all models had relatively high expression of *LIN28B*, only the more carcinomatous models expressed high levels of *MYCN* (PH419, PH142, and PH006), compared to the TCGA-OV cohort (Figure 3b). By Western blot, expression of the mesenchymal markers ZEB1, N-cadherin and vimentin varied between models. There was a trend towards higher ZEB1 and vimentin expression in the more sarcomatous models, with the exception of PH003mixed, which expressed very low levels of ZEB1. N-cadherin was highly expressed in most models and HMGA2 was expressed at similar levels in all models (Figure 3d). EMT scores were more representative of pathology (i.e. degree of mesenchymal characteristics) than any of the individual mesenchymal markers assessed by Western blotting.

Platinum-based chemotherapy is ineffective in OCS PDX

In vivo, 4/6 PDX were refractory to cisplatin, based on our previous criteria (40) (Figure 4a and Supplementary Figure S8). Initial tumour regression was observed in PH142 and #1040 but PD occurred by day 42 and day 60 respectively, defining both as cisplatin resistant (40) (Table 2).

Microtubule-targeting agents paclitaxel, vinorelbine and eribulin are effective in OCS

Microtubule-targeting agents induced tumour regression and showed an improvement of median TTH in most OCS PDX models. 3/6 PDX (#1040, PH419 and PH006) were classified as sensitive to paclitaxel according to the same criteria used for cisplatin (40), 2/6 were resistant (PH142 and PH592) and 1/6 was refractory (PH003; *in vivo* long-term treatment data was obtained for the PH003mixed model prior to development of the PH003sarc model) (Figure 4a and Supplementary Figure S8). Indeed, 5/6 models displayed an improvement in median TTH compared with vehicle, with 4/6 models also displaying an improvement in median TTH compared with cisplatin (Table 2).

The same 3/6 OCS PDX (#1040, PH142 and PH006) were sensitive to vinorelbine, with 2/6 being resistant (PH419 and PH592) and PH003 again being refractory (Figure 4a and Supplementary Figure S8). The more sarcomatous PDX models, PH003 and PH592, were less sensitive to vinorelbine than the more carcinomatous models. Significant improvements in median TTH compared with vehicle were observed for 5/6 models, and in 4/6 models compared with cisplatin (Table 2).

Lastly, the same 3/6 PDX models (#1040, PH419 and PH006) were sensitive to eribulin treatment, showing near complete responses. 2/6 were resistant (PH142 and PH592) and PH003 was again refractory (Figure 4a and Supplementary Figure S8). Significant improvements in median TTH compared to vehicle and cisplatin were observed for 5/6 and 4/6 models, respectively (Table 2). Eribulin treatment of PH592, which was predominantly sarcomatous, resulted in significant tumour stabilisation to 40 days followed by marked tumour regression between days 60 to 80 before rapid disease progression. Even for the most aggressive model, PH003, eribulin treatment resulted in a statistically significant improvement in median TTH, albeit of short duration (8 days (vehicle) vs 25 days (eribulin) (p=0.0003) and 15 days (cisplatin) vs 25 days (eribulin) (p=0.0044)) (Table 2).

Over time, a new lineage of the sarcomatous PDX PH592 (PH592-B) arose, which was markedly more sensitive to both cisplatin (median TTH of 15 days (PH592-A) vs 71 days (PH592-B); p<0.0001) and eribulin (92 days (PH592-A) vs 102 days (PH592-B); p=0.0240) (Supplementary Figure S9 and Supplementary Table S19) than the sister lineage PH592-A.

In vivo eribulin treatment reduces the expression of mesenchymal markers, including HMGA2, in OCS PDX tumours

PDX tumours were harvested one week after mice received a single dose of eribulin (or vehicle control) and expression of EMT markers was assessed by IHC and Western blot. Eribulin reduced expression of the mesenchymal marker HMGA2 as well as ZEB1 and N-cadherin in 6/7 and 5/7 models, respectively (Figures 4b-d; Supplementary Figure S10). Expression of ZEB1 was generally unchanged in 7/7 models following cisplatin treatment (Supplementary Figure S11a).

Genes involved in cholesterol biosynthesis and immune recognition are differentially expressed in OCS PDX tumours following eribulin treatment

RNAseq analysis of PDX tumours harvested one week after a single dose of eribulin (Supplementary Table S16) indicated significant down-regulation of genes related to the Gene Ontology (GO) terms “protein targeting to membrane”, “translational initiation”, and “regulation of cholesterol biosynthesis”, and up-regulation of genes related to the GO term “immune activation” (Figure 5a; Supplementary Tables S20-S23). Interestingly, significantly down-regulated genes included eleven involved in cholesterol biosynthesis, cholesterol uptake or cholesterol transport: *SREBF2*, *HMGCR*, *HMGCS1*, *MVK*, *LDLR*, *INSIG1*, *IDI1*, *FDFT1*,

MSMO1, *CYP51A1*, *STARD4*. Expression of hydroxymethylglutaryl-CoA synthase (HMGCS) and squalene epoxidase (SQLE), key components of the mevalonate (MVA) pathway involved in cholesterol biosynthesis, as well as the low density lipoprotein receptor (LDLR), which mediates cellular uptake of exogenous cholesterol, was reduced in 4/7 models (PH419, PH142, PH592-A and PH592-B) following eribulin treatment. Expression of SQLE was also significantly reduced in the PH003sarc model and N-MYC expression, which appears to indicate sensitivity to eribulin, was significantly reduced in 4/5 N-MYC-positive models following eribulin treatment (Figures 5b and c). Interestingly, expression of HMGCS, SQLE and LDLR was also reduced in 1/7 model (PH142) following cisplatin treatment. Unlike for eribulin treatment, this response was restricted to the PH142 model, with expression being generally unchanged in 6/7 models following cisplatin treatment (Supplementary Figure S11a).

Eribulin treatment down-regulates the mevalonate pathway and induces infiltration of CD8-positive T-cells in OCS PDX models

To test whether cholesterol levels decreased in OCS tumours in response to eribulin treatment the amount of cholesterol was quantified in PDX tumours. Surprisingly, total cholesterol levels were found to increase almost two-fold in 3/7 models (PH419, PH592-A and PH592-B), and slightly in 2/7 models (PH142 and PH003sarc) (Figure 5d). The tumours with increased levels of cholesterol following eribulin treatment were the same tumours that displayed down-regulation of the MVA pathway (Figure 5b and 5c). Cholesterol levels were also significantly increased in 1/7 model (PH142) following cisplatin treatment, correlating with down-regulation of the MVA pathway observed in this model (Supplementary Figure S11b). Cholesterol levels were also slightly increased in PH419 tumours following cisplatin treatment, although not as dramatically as had been observed following eribulin treatment (Supplementary Figure S11b). Total cellular cholesterol includes free cholesterol as well as cholesterol esters. In eribulin-responsive/N-MYC-positive PH419, increased total cholesterol was equally accounted for by both free cholesterol and cholesterol ester (Figure 5d). Oil Red O staining indicated that eribulin-treated PH419 tumours had more esterified cholesterol within lipid deposits than did vehicle treated tumours (Figure 5e). While a modest increase in lipid deposits were observed in PH142 tumours following both eribulin and cisplatin treatment, increases were more dramatic following eribulin treatment (Supplementary Figure S11c). This effect was also specific to the models where increased cholesterol levels had previously been observed, as no increased lipid deposits were observed in PH006 tumours (Supplementary Figure S11c).

To investigate this mechanism further, we generated a cell line from a PH419 tumour. Cells were plated on collagen, treated with eribulin, and harvested at indicated time-points. Expression of the mesenchymal markers ZEB1 and N-cadherin was reduced after four days of eribulin treatment and this effect was maintained at seven days (Figure 5f). Expression of the early MVA pathway enzyme HMGCS was unaffected by eribulin treatment. In contrast, expression of the late MVA pathway enzyme SQLE, as well as the receptor for cholesterol uptake LDLR, was reduced after four days of eribulin treatment and this effect was maintained at seven days (Figure 5f). Interestingly, total cholesterol levels were significantly increased 48 hours after eribulin treatment, confirming that MVA pathway down-regulation occurred after cholesterol accumulation (Figure 5g). We quantified cholesterol in a second cell line generated from a PH142 tumour with similar results (Supplementary Figure S11d). As expected, based on the results from the tumours, we also saw a maintained increase in cholesterol in PH142 cells following cisplatin treatment (Supplementary Figure S11d).

To investigate cell death following treatment, we treated OCS cells with cisplatin or eribulin and harvested cells at 48 hours to look at the percentage of cells positive for Annexin V and/or PI. As was observed in the tumours, PH142 cells were more sensitive to cisplatin than PH419 cells (Supplementary Figure S12a). Eribulin was unable to induce greater than 30% cell death in either cell line, even at doses more than 1000 fold that which induced cholesterol accumulation (Supplementary Figure S12a). Consequently, expression of cleaved-PARP-1and cleaved-caspase 3 could be detected in cells treated with cisplatin but not those treated with eribulin (Supplementary Figure S12b). Senescence assays were also carried out and indeed PH142 cells produced β-galactosidase following treatment with eribulin but not cisplatin (Supplementary Figure S12c). While PH419 cells did not produce β-galactosidase following eribulin treatment, they resembled senescent cells and appeared to have lost replicative capacity, a phenomenon we have previously observed in cancer cells treated with microtubule inhibitors (41).

Further analysis of the gene expression data obtained from the 18 cases in our OCS cohort, estimated they have fewer CD8-positive T-cells than tumours in the TCGA-OV cohort (Supplementary Figure S13). To investigate whether eribulin treatment could induce an immune response, as suggested by the gene expression data from the treated PDX models, we grew two additional OCS PDX models (#1105 and #1177) in mice harbouring a human

immune system (HIS) (Figure 6a, Supplementary Table S24). PDX tumours were harvested one week after mice received a single dose of eribulin, cisplatin or vehicle control, and CD8-positive T-cells were detected by IHC (Figure 6b). 2/2 models exposed to eribulin had a significantly greater percentage of CD8-positive T-cells than control tumours (p=0.005 and <0.0001 for #1105 and #1177, respectively; Figure 6c). A significant increase in the percentage of CD8-positive T-cells was also observed following cisplatin treatment in 1/2 models (#1105, p<0.0001; Figure 6c).

Discussion

OCS is a rare, heterogeneous and clinically aggressive cancer, with poorer overall survival than HGSC despite a similar mutation and copy number profile (42). The biphasic nature of OCS and a poor understanding of how these tumours develop has hindered development of effective treatment options. Two recent studies performed whole exome sequencing on separated components of OCS tumours, but on no more than four tumours each (8,9). Here, we analysed 377 genes (for mutations, copy number, or both) in 18 OCS tumours where the carcinomatous and sarcomatous components were analysed independently along with associated metastases, where available. We found mutations commonly identified in OCS, with the initial or truncal mutation likely to occur in *TP53*. In all of the cases, the same *TP53* mutation was identified in all sites available; carcinoma, sarcoma and metastasis, suggesting strongly that OCS tumours in our cohort were monoclonal. Furthermore, we carried out RNAseq analysis, which has not previously been achieved for the independent components in OCS. The carcinomatous component was found to have a significantly higher EMT score than conventional HGSC, indicating these tumours may have been primed to undergo sarcomatous transformation early in carcinogenesis. Together, these data indicate EMT plays a key role in OCS tumorigenesis and support the conversion theory for OCS histogenesis. This study also highlights the potential downfall of treating women with OCS in the same way as HGSC, as we have shown that despite the genomic similarity, OCS are phenotypically distinct, particularly with regard to drug responses and mesenchymal characteristics.

Significant up-regulation of *LIN28B* and *HMGA2* in our cohort of 18 OCS tumours compared to HGSC suggest that the N-MYC/LIN28B pathway is important in the development and maintenance of OCS. Using this knowledge, we developed a GEMM of OCS by overexpressing *Lin28b* and inhibiting p53 in PAX8$^+$ FTSECs. While the OCS GEMM tumours

exhibited high expression of *Lin28b* and *Mycn*, the derived cell line displayed high expression of *Lin28b* and *Hmga2*, indicating that we had generated two closely related preclinical models of OCS. This demonstrates the complexity of the N-MYC pathway, as was also indicated by the RNAseq data from our patient samples. Observed expression of this pathway depends on multiple feedback loops and influences from outside the pathway, such as by transcription factors, with influences occurring at the level of transcription and translation, frequently resulting in complex relationships (43).

These models were used to compare the current standard-of-care treatments for OCS with novel treatments, including the unique microtubule-targeting drug eribulin, which has been shown to reverse EMT (29) and has demonstrated efficacy against metastatic breast cancer, soft-tissue sarcoma and non-small cell lung cancer (NSCLC) (30-33). While the GEMM tumours were refractory to cisplatin, paclitaxel and PLD *in vivo*, they were responsive to vinorelbine and eribulin. After just a single dose of eribulin, a notable decrease in tumour cell proliferation was observed. *In vitro*, eribulin significantly reduced adhesion, invasion and branching in 3D cultres. Finally, an impressive reduction in expression of the mesenchymal markers HMGA2, ZEB1, N-cadherin, and vimentin was observed in GEMM cells, indicating eribulin could reverse EMT in these cells.

A cohort of molecularly annotated OCS PDX models was found to have higher EMT scores than HGSC with the most carcinomatous model, PH419, having the lowest EMT score and the most sarcomatous model, PH003sarc, having the highest. At the protein level, PH003sarc also had the highest expression of the mesenchymal markers N-cadherin and vimentin. Interestingly, the two models containing mixed cells, PH142 and PH006, also had high expression of N-cadherin, vimentin and ZEB1. This matched their high EMT scores obtained from RNAseq data and indicated that pathology alone was insufficient to determine the level of sarcomatous transformation occurring in each OCS model.

Anti-microtubule agents were more effective than platinum-based chemotherapy in our OCS PDX cohort. The proportion of carcinoma correlated with cisplatin sensitivity, where the more carcinomatous PDX had some initial response, whilst the most sarcomatous PDX were completely refractory. Responses were observed for almost all PDX to the microtubule-targeting drugs paclitaxel, vinorelbine and eribulin. With metastases more commonly comprising carcinoma cells, this suggests that eribulin would also inhibit progression and

metastasis. PDX PH003 was the exception, where tumours were refractory to all treatment regimens tested. This drug-refractory PDX was found to lack N-MYC expression, representing a particularly aggressive subtype of OCS, corresponding to rapidly progressive disease in the patient (44). PH952-A, the more drug-resistant lineage of PH592, had almost undetectable levels of N-MYC, whereas it was expressed in the more drug sensitive lineage, PH592-B, supporting our hypothesis that N-MYC correlates with sensitivity to eribulin. We observed a decrease in HMGA2, N-cadherin and ZEB1 expression in most models following a single dose of eribulin. We hypothesised that eribulin interfered with the N-MYC pathway, leading to a reduction in the mesenchymal characteristics of OCS, including down-regulation of HMGA2. Indeed, we later discovered that eribulin reduced the expression of N-MYC in N-MYC-expressing tumours, with the exception of PH592-B. As has been seen for MYC (45,46), we hypothesise that N-MYC associates with microtubules to facilitate nuclear translocation and stabilisation, which may be affected by microtubule inhibitors, such as eribulin. Despite PH419 being the most carcinomatous model, it was still found to express the mesenchymal markers ZEB1, N-cadherin and HMGA2, which were all reduced following eribulin treatment. This model was also found to have a higher EMT score than most HGSC tumours, and so it was not surprising that this model was also significantly sensitive to eribulin treatment. Ultimately, we found eribulin to be very effective in most of our OCS models, indicating it should be offered to OCS patients as an alternative therapeutic to carboplatin and paclitaxel. As has been seen in locally advanced and metastatic breast cancer (47), we hypothesise that eribulin will improve survival of OCS patients with a manageable toxicity profile.

We found that eribulin treatment also resulted in a significant reduction in the expression of genes in the MVA pathway and a significant up-regulation of genes involved in immune activation. Activation of the MVA pathway has previously been observed in *MYCN* amplified neuroblastoma, with apparent reliance of these tumours on this pathway for survival (48). We hypothesise that N-MYC is a key driver of OCS, implicating the MVA pathway in OCS cell survival and drug resistance. Notably, the most aggressive PDX model PH003mixed, which displayed no change in expression of MVA pathway proteins after eribulin treatment, also had very low expression of *MYCN* by RNAseq and expression of N-MYC was undetectable by western blot, further supporting our hypothesis that N-MYC expression confers sensitivity to eribulin. On the other hand, one of the most sensitive PDX models PH006, which also displayed no change in expression of MVA pathway proteins after eribulin treatment, had very high expression of N-MYC by RNAseq and western blot. It is possible that changes in

cholesterol levels and MVA pathway activity in this model may be evident at another time-point. Supporting the RNAseq data, we saw a reduction in the expression of HMGCS, SQLE and LDLR in 4/7 PDX models: PH419, PH142, PH592-A and PH592-B. SQLE expression was also reduced in the PH003sarc model. Strikingly, cholesterol levels were increased in the 4/7 PDX in which we had observed a down-regulation of MVA pathway proteins. Previously, a study of drugs that could inhibit EMT in breast cancer cells also observed an increase in cellular cholesterol levels following treatment (49). Increased intracellular cholesterol was found to reduce membrane fluidity, leading to a reversal of EMT characteristics, as we have observed in this study. Whilst cholesterol plays an important role in regulating the properties of cell membranes, too much cellular cholesterol can also be toxic (50). We hypothesised that as cholesterol reached toxic levels as a result of eribulin treatment, negative feedback regulation of the MVA pathway took place to lower cholesterol levels. This down-regulation of the MVA pathway is of particular interest, as it has previously been associated with an improved response to anti-cancer drugs and reduced development of drug resistance (reviewed in (51)). We confirmed this order of events using a PH419 primary cell line, where cholesterol levels were significantly increased 48 hours after eribulin treatment, resulting in reduced EMT indicated by a decreased expression of ZEB1 and N-cadherin, and followed by down-regulation of SQLE and LDLR expression at 96 hours. With respect to OCS, this protective response may come too late, with cell death, growth inhibition and tumour regression resulting from eribulin treatment in many cases. We also observed significantly increased cholesterol accumulation following cisplatin treatment in the PH142 model. Interestingly, this model is the most sensitive to cisplatin treatment, likely due to harbouring a *BRCA2* mutation. While cholesterol accumulation and subsequent MVA pathway down-regulation occured when OCS responded to other anti-cancer drugs, such as cisplatin, this process was more striking following eribulin treatment. Importantly, EMT reversal was not observed following cisplatin treatment, and tumour remission was not as deep or as long-lasting compared to eribulin treatment.

Cholesterol accumulation has been found to induce an immune response in cancer via multiple mechanisms, such as through enhancing inflammation signalling pathways or inducing antigen presentation (52). Indeed, in our OCS PDX models, we also observed a significant increase in the expression of genes involved in immune responses following eribulin treatment, such as *TLR7* and *IRF8*, which have independently been associated with increased inflammation and recruitment of tumour infiltrating lymphocytes in different cancer types (53,54). Indeed, we observed increased numbers of CD8-positive T-cells in tumours following eribulin treatment,

indicating activation of an immune response. Furthermore, a recent study linked *MYCN* overexpression in neuroblastoma to cancer immune evasion (55). Thus, we have found that eribulin can initiate anti-tumour immune responses in OCS, as has been observed in other tumour types treated with eribulin (56). We have also discovered that OCS tumours that are sensitive to eribulin treatment exhibit an accumulation of cholesterol, which may be responsible for instigating these observed immune responses. Ultimately, we hypothesise that eribulin elicits its strong anti-tumour effects in OCS through a combination of EMT reversal, MVA pathway down-regulation and induction of an immune response. Therefore, early phase clinical trials in OCS of eribulin as a single agent or in combination with immunotherapy, should be initiated to improve treatment options for women with OCS.

Acknowledgements

This work was supported by fellowships and grants from the National Health and Medical Research Council (NHMRC Australia; Project Grants 1062702, 1081178 (CLS) and 1104348 (MJW, DDB, ATP and CLS), Senior Research Fellowship 1116955 (ATP), Investigator Grant 2008692 (JEV), Ideas Grant 1183070 (JEV)); the Stafford Fox Medical Research Foundation (ELK, JB, CJV, RL, ATP, CLS and HEB); the Lorenzo and Pamela Galli Medical Research Trust (ATP); Cancer Council Victoria (Sir Edward Dunlop Fellowship in Cancer Research (CLS) and Ovarian Cancer Research Grant-in-Aid 1186314 (GR, CJV, AF and HEB); the Victorian Cancer Agency (Clinical Fellowships CRF10-20, CRF16014 (CLS), Early Career Research Fellowship ECRF19003 (GD)); Herman Trust University of Melbourne (CLS); CRC Cancer Therapeutics (Grant support (CLS), PhD top-up scholarship (GYH)); Australian Commonwealth Government and the University of Melbourne (Research Training Program Scholarship (GYH and AH)); Cancer Research UK Cambridge Institute Studentship; Cambridge Poynton Scholarship; Cambridge Trust International Scholarship (PhD funding for ELK); Research funding from Eisai (CLS and HEB).

The Scottish Genomes Partnership is funded by the Chief Scientist Office of the Scottish Government Health Directorates (grant reference SGP/1) and The Medical Research Council Whole Genome Sequencing for Health and Wealth Initiative. Additional funding was provided by the Medical Research Council (the Glasgow Molecular Pathology Node, grant reference MR/N005813/1), Cancer Research UK (grant references A15973 (IMcN) and A17263 (AVB)), the Wellcome Trust (grant reference 103721/Z/14/Z (AVB)) and the Beatson Cancer Charity (grant reference 15-16-051 (IMcN and PR)), the Imperial NIHR Biomedical Research Centre

(grant references PSC593 and P77646 (IMcN, DPE, HBM)) and Ovarian Cancer Action (grant reference P76567 (IMcN, DPE, HBM)).

We thank Silvia Stoev, Rachel Hancock, and Kathy Barber for technical assistance. We thank Prof Ronny Drapkin, Prof Jane Visvader (and Osaka Bioscience Institute, Japan), and Prof Johannes H. Schulte for kind gifts of the mouse strains used to generate the GEMM. We thank Dr Paul Haluska (Mayo Clinic, USA) for the cryopreserved PDX material used to re-establish PDXs PH419, PH142, PH006, PH003 and PH592 within our laboratory. We thank Eisai Co., Ltd. for supply of eribulin. We thank Prof Elizabeth Swisher and Dr Marc Radke for the BROCA sequencing of case #1040, Prof Sean Grimmond and Dr Joep Vissers for WGS of cases #1105 and #1177, and Andrew Fellowes for the TSO500 sequencing of cases PH142, PH003 and PH006. We thank Jocelyn Penington for data deposition to EGA. This work was made possible through the Australian Cancer Research Foundation, the Victorian State Government Operational Infrastructure Support and Australian Government NHMRC IRIISS. The Australian Ovarian Cancer Study Group was supported by the U.S. Army Medical Research and Materiel Command under DAMD17-01-1-0729, The Cancer Council Victoria, Queensland Cancer Fund, The Cancer Council New South Wales, The Cancer Council South Australia, The Cancer Council Tasmania and The Cancer Foundation of Western Australia (Multi-State Applications 191, 211 and 182) and the National Health and Medical Research Council of Australia (NHMRC; ID199600; ID400413 and ID400281). The Australian Ovarian Cancer Study gratefully acknowledges additional support from Ovarian Cancer Australia and the Peter MacCallum Foundation. The AOCS also acknowledges the cooperation of the participating institutions in Australia and acknowledges the contribution of the study nurses, research assistants and all clinical and scientific collaborators to the study. The complete AOCS Study Group can be found at www.aocstudy.org. Support was also provided by Ovarian Cancer Action, the Cancer Research UK Centres and Experimental Cancer Medicine Centres at both Glasgow and Imperial and the NIHR Imperial Biomedical Research Centre. We would like to thank all of the women who participated in these research programs.

Author contributions

C.L.S., M.J.W., I.A.M., H.E.B, and A.T.P. designed the study, developed methodology, analysed data, wrote the manuscript and supervised the study. G.Y.H., E.L.K. and H.E.B. conceived/performed experiments, analysed data, and wrote the manuscript. J.B. analysed data, supervised the study and reviewed the manuscript. E.L., C.J.V. and O.K., developed

methodology, performed experiments, analysed data and reviewed the manuscript. D.P.E., R.U.-G., U.-M.B., S.D., G.B., A.F., A.H, R.L., G.D, J.V., N.K.C. and G.R. conceived/performed experiments and reviewed the manuscript. H.B.M. analysed data, wrote and reviewed the manuscript. P.R., R.M.G. and A.V.B. supervised the study and reviewed the manuscript. S.L.C designed the study, developed methodology, analysed data, supervised the study and reviewed the manuscript. O.McN., A. DeF., J.W. and D.D.B. acquired data or samples, supervised the study and reviewed the manuscript. N.T. acquired data, provided administrative support and reviewed the manuscript. AOCS acquired data and reviewed the manuscript.

Uncategorized References

1. Rauh-Hain JA, Gonzalez R, Bregar AJ, Clemmer J, Hernandez-Blanquisett A, Clark RM, *et al.* Patterns of care, predictors and outcomes of chemotherapy for ovarian carcinosarcoma: A National Cancer Database analysis. Gynecol Oncol **2016**;142:38-43
2. Mano MS, Rosa DD, Azambuja E, Ismael G, Braga S, D'Hondt V, *et al.* Current management of ovarian carcinosarcoma. Int J Gynecol Cancer **2007**;17:316-24
3. Rauh-Hain JA, Birrer M, Del Carmen MG. "Carcinosarcoma of the ovary, fallopian tube, and peritoneum: Prognostic factors and treatment modalities". Gynecol Oncol **2016**;142:248-54
4. Abeln EC, Smit VT, Wessels JW, de Leeuw WJ, Cornelisse CJ, Fleuren GJ. Molecular genetic evidence for the conversion hypothesis of the origin of malignant mixed mullerian tumours. J Pathol **1997**;183:424-31
5. Growdon WB, Roussel BN, Scialabba VL, Foster R, Dias-Santagata D, Iafrate AJ, *et al.* Tissue-specific signatures of activating PIK3CA and RAS mutations in carcinosarcomas of gynecologic origin. Gynecol Oncol **2011**;121:212-7
6. Jin Z, Ogata S, Tamura G, Katayama Y, Fukase M, Yajima M, *et al.* Carcinosarcomas (malignant mullerian mixed tumors) of the uterus and ovary: a genetic study with special reference to histogenesis. Int J Gynecol Pathol **2003**;22:368-73
7. Kounelis S, Jones MW, Papadaki H, Bakker A, Swalsky P, Finkelstein SD. Carcinosarcomas (malignant mixed mullerian tumors) of the female genital tract: comparative molecular analysis of epithelial and mesenchymal components. Hum Pathol **1998**;29:82-7
8. Gotoh O, Sugiyama Y, Takazawa Y, Kato K, Tanaka N, Omatsu K, *et al.* Clinically relevant molecular subtypes and genomic alteration-independent differentiation in gynecologic carcinosarcoma. Nat Commun **2019**;10:4965
9. Zhao S, Bellone S, Lopez S, Thakral D, Schwab C, English DP, *et al.* Mutational landscape of uterine and ovarian carcinosarcomas implicates histone genes in epithelial-mesenchymal transition. Proc Natl Acad Sci U S A **2016**;113:12238-43
10. del Carmen MG, Birrer M, Schorge JO. Carcinosarcoma of the ovary: a review of the literature. Gynecol Oncol **2012**;125:271-7
11. Barker HE, Scott CL. Genomics of gynaecological carcinosarcomas and future treatment options. Semin Cancer Biol **2020**

12. Fujii H, Yoshida M, Gong ZX, Matsumoto T, Hamano Y, Fukunaga M, *et al.* Frequent genetic heterogeneity in the clonal evolution of gynecological carcinosarcoma and its influence on phenotypic diversity. Cancer Res **2000**;60:114-20
13. Jones S, Stransky N, McCord CL, Cerami E, Lagowski J, Kelly D, *et al.* Genomic analyses of gynaecologic carcinosarcomas reveal frequent mutations in chromatin remodelling genes. Nat Commun **2014**;5:5006
14. Morishita A, Zaidi MR, Mitoro A, Sankarasharma D, Szabolcs M, Okada Y, *et al.* HMGA2 is a driver of tumor metastasis. Cancer Res **2013**;73:4289-99
15. Gattas GJ, Quade BJ, Nowak RA, Morton CC. HMGIC expression in human adult and fetal tissues and in uterine leiomyomata. Genes Chromosomes Cancer **1999**;25:316-22
16. Rogalla P, Drechsler K, Frey G, Hennig Y, Helmke B, Bonk U, *et al.* HMGI-C expression patterns in human tissues. Implications for the genesis of frequent mesenchymal tumors. Am J Pathol **1996**;149:775-9
17. Chang KP, Lin SJ, Liu SC, Yi JS, Chien KY, Chi LM, *et al.* Low-molecular-mass secretome profiling identifies HMGA2 and MIF as prognostic biomarkers for oral cavity squamous cell carcinoma. Sci Rep **2015**;5:11689
18. Piscuoglio S, Zlobec I, Pallante P, Sepe R, Esposito F, Zimmermann A, *et al.* HMGA1 and HMGA2 protein expression correlates with advanced tumour grade and lymph node metastasis in pancreatic adenocarcinoma. Histopathology **2012**;60:397-404
19. Saada-Bouzid E, Burel-Vandenbos F, Ranchere-Vince D, Birtwisle-Peyrottes I, Chetaille B, Bouvier C, *et al.* Prognostic value of HMGA2, CDK4, and JUN amplification in well-differentiated and dedifferentiated liposarcomas. Mod Pathol **2015**;28:1404-14
20. Sun M, Gomes S, Chen P, Frankenberger CA, Sankarasharma D, Chung CH, *et al.* RKIP and HMGA2 regulate breast tumor survival and metastasis through lysyl oxidase and syndecan-2. Oncogene **2014**;33:3528-37
21. Wang X, Liu X, Li AY, Chen L, Lai L, Lin HH, *et al.* Overexpression of HMGA2 promotes metastasis and impacts survival of colorectal cancers. Clin Cancer Res **2011**;17:2570-80
22. Park SM, Shell S, Radjabi AR, Schickel R, Feig C, Boyerinas B, *et al.* Let-7 prevents early cancer progression by suppressing expression of the embryonic gene HMGA2. Cell Cycle **2007**;6:2585-90
23. Helland A, Anglesio MS, George J, Cowin PA, Johnstone CN, House CM, *et al.* Deregulation of MYCN, LIN28B and LET7 in a molecular subtype of aggressive high-grade serous ovarian cancers. PLoS One **2011**;6:e18064
24. Wang T, Wang G, Hao D, Liu X, Wang D, Ning N, *et al.* Aberrant regulation of the LIN28A/LIN28B and let-7 loop in human malignant tumors and its effects on the hallmarks of cancer. Mol Cancer **2015**;14:125
25. Tothill RW, Tinker AV, George J, Brown R, Fox SB, Lade S, *et al.* Novel molecular subtypes of serous and endometrioid ovarian cancer linked to clinical outcome. Clin Cancer Res **2008**;14:5198-208
26. Mahajan A, Liu Z, Gellert L, Zou X, Yang G, Lee P, *et al.* HMGA2: a biomarker significantly overexpressed in high-grade ovarian serous carcinoma. Mod Pathol **2010**;23:673-81
27. Funahashi Y, Okamoto K, Adachi Y, Semba T, Uesugi M, Ozawa Y, *et al.* Eribulin mesylate reduces tumor microenvironment abnormality by vascular remodeling in preclinical human breast cancer models. Cancer Sci **2014**;105:1334-42

28. Kashiwagi S, Asano Y, Goto W, Takada K, Takahashi K, Noda S, *et al.* Use of Tumor-infiltrating lymphocytes (TILs) to predict the treatment response to eribulin chemotherapy in breast cancer. PLoS One **2017**;12:e0170634
29. Yoshida T, Ozawa Y, Kimura T, Sato Y, Kuznetsov G, Xu S, *et al.* Eribulin mesilate suppresses experimental metastasis of breast cancer cells by reversing phenotype from epithelial-mesenchymal transition (EMT) to mesenchymal-epithelial transition (MET) states. Br J Cancer **2014**;110:1497-505
30. Cortes J, O'Shaughnessy J, Loesch D, Blum JL, Vahdat LT, Petrakova K, *et al.* Eribulin monotherapy versus treatment of physician's choice in patients with metastatic breast cancer (EMBRACE): a phase 3 open-label randomised study. Lancet **2011**;377:914-23
31. Katakami N, Felip E, Spigel DR, Kim JH, Olivo M, Guo M, *et al.* A randomized, open-label, multicenter, phase 3 study to compare the efficacy and safety of eribulin to treatment of physician's choice in patients with advanced non-small cell lung cancer. Ann Oncol **2017**;28:2241-7
32. Kaufman PA, Awada A, Twelves C, Yelle L, Perez EA, Velikova G, *et al.* Phase III open-label randomized study of eribulin mesylate versus capecitabine in patients with locally advanced or metastatic breast cancer previously treated with an anthracycline and a taxane. J Clin Oncol **2015**;33:594-601
33. Schoffski P, Chawla S, Maki RG, Italiano A, Gelderblom H, Choy E, *et al.* Eribulin versus dacarbazine in previously treated patients with advanced liposarcoma or leiomyosarcoma: a randomised, open-label, multicentre, phase 3 trial. Lancet **2016**;387:1629-37
34. Wakefield M. Xenomapper: Mapping reads in a mixed species context. **2016**;The Journal of Open Source Software:18
35. Harrison PF, Pattison AD, Powell DR, Beilharz TH. Topconfects: a package for confident effect sizes in differential expression analysis provides a more biologically useful ranked gene list. Genome Biol **2019**;20:67
36. Wakefield MJ. Survival volume: interactive volume threshold survival graphs. The Journal of Open Source Software **2016**;1(8):111
37. Barker HE, Chang J, Cox TR, Lang G, Bird D, Nicolau M, *et al.* LOXL2-mediated matrix remodeling in metastasis and mammary gland involution. Cancer Res **2011**;71:1561-72
38. Sreenan JJ, Hart WR. Carcinosarcomas of the female genital tract. A pathologic study of 29 metastatic tumors: further evidence for the dominant role of the epithelial component and the conversion theory of histogenesis. Am J Surg Pathol **1995**;19:666-74
39. Chiyoda T, Tsuda H, Tanaka H, Kataoka F, Nomura H, Nishimura S, *et al.* Expression profiles of carcinosarcoma of the uterine corpus-are these similar to carcinoma or sarcoma? Genes Chromosomes Cancer **2012**;51:229-39
40. Topp MD, Hartley L, Cook M, Heong V, Boehm E, McShane L, *et al.* Molecular correlates of platinum response in human high-grade serous ovarian cancer patient-derived xenografts. Mol Oncol **2014**;8:656-68
41. Barker HE, Patel R, McLaughlin M, Schick U, Zaidi S, Nutting CM, *et al.* CHK1 Inhibition Radiosensitizes Head and Neck Cancers to Paclitaxel-Based Chemoradiotherapy. Mol Cancer Ther **2016**;15:2042-54
42. Brackmann M, Stasenko M, Uppal S, Erba J, Reynolds RK, McLean K. Comparison of first-line chemotherapy regimens for ovarian carcinosarcoma: a single institution case series and review of the literature. BMC Cancer **2018**;18:172

43. Balzeau J, Menezes MR, Cao S, Hagan JP. The LIN28/let-7 Pathway in Cancer. Front Genet **2017**;8:31
44. Glaser G, Weroha SJ, Becker MA, Hou X, Enderica-Gonzalez S, Harrington SC, *et al.* Conventional chemotherapy and oncogenic pathway targeting in ovarian carcinosarcoma using a patient-derived tumorgraft. PLoS One **2015**;10:e0126867
45. Becker S, Kiecke C, Schafer E, Sinzig U, Deuper L, Trigo-Mourino P, *et al.* Destruction of a Microtubule-Bound MYC Reservoir during Mitosis Contributes to Vincristine's Anticancer Activity. Mol Cancer Res **2020**;18:859-72
46. Alexandrova N, Niklinski J, Bliskovsky V, Otterson GA, Blake M, Kaye FJ, *et al.* The N-terminal domain of c-Myc associates with alpha-tubulin and microtubules in vivo and in vitro. Mol Cell Biol **1995**;15:5188-95
47. Tanni KA, Truong CB, Johnson BS, Qian J. Comparative effectiveness and safety of eribulin in advanced or metastatic breast cancer: a systematic review and meta-analysis. Crit Rev Oncol Hematol **2021**;163:103375
48. Liu M, Xia Y, Ding J, Ye B, Zhao E, Choi JH, *et al.* Transcriptional Profiling Reveals a Common Metabolic Program in High-Risk Human Neuroblastoma and Mouse Neuroblastoma Sphere-Forming Cells. Cell Rep **2016**;17:609-23
49. Zhao W, Prijic S, Urban BC, Tisza MJ, Zuo Y, Li L, *et al.* Candidate Antimetastasis Drugs Suppress the Metastatic Capacity of Breast Cancer Cells by Reducing Membrane Fluidity. Cancer Res **2016**;76:2037-49
50. Tabas I. Consequences of cellular cholesterol accumulation: basic concepts and physiological implications. J Clin Invest **2002**;110:905-11
51. Abdulla N, Vincent CT, Kaur M. Mechanistic Insights Delineating the Role of Cholesterol in Epithelial Mesenchymal Transition and Drug Resistance in Cancer. Front Cell Dev Biol **2021**;9:728325
52. Huang B, Song BL, Xu C. Cholesterol metabolism in cancer: mechanisms and therapeutic opportunities. Nat Metab **2020**;2:132-41
53. Zhang M, Yan Z, Wang J, Yao X. Toll-like receptors 7 and 8 expression correlates with the expression of immune biomarkers and positively predicts the clinical outcome of patients with melanoma. Onco Targets Ther **2017**;10:4339-46
54. Gatti G, Betts C, Rocha D, Nicola M, Grupe V, Ditada C, *et al.* High IRF8 expression correlates with CD8 T cell infiltration and is a predictive biomarker of therapy response in ER-negative breast cancer. Breast Cancer Res **2021**;23:40
55. Raieli S, Di Renzo D, Lampis S, Amadesi C, Montemurro L, Pession A, *et al.* MYCN Drives a Tumor Immunosuppressive Environment Which Impacts Survival in Neuroblastoma. Front Oncol **2021**;11:625207
56. Goto W, Kashiwagi S, Asano Y, Takada K, Morisaki T, Fujita H, *et al.* Eribulin Promotes Antitumor Immune Responses in Patients with Locally Advanced or Metastatic Breast Cancer. Anticancer Res **2018**;38:2929-38

Tables

Table 1: *In vivo* responses of GEMM tumours to cisplatin, paclitaxel, pegylated liposomal doxorubicin (PLD), vinorelbine and eribulin

Treatment	Number of mice (n)	Time to PD (days)	Median TTH (days)	p value Compared to vehicle	p value Compared to cisplatin	p value Compared to eribulin	p value Compared to paclitaxel	p value Compared to doxorubicin liposomal	p value Compared to vinorelbine	Drug response score
Vehicle	25	7	15							

Cisplatin	10	7	18	0.03		0.2	0.9		<0.0001	Refractory
Paclitaxel	3	7	36	0.01	0.9	0.007		0.5	0.0006	Refractory
PLD	3	7	29	0.08	0.6	0.004	0.5		0.0002	Refractory
Vinorelbine	9	56	81	<0.0001	<0.0001	0.001	0.0006	0.0002		Responsive
Eribulin	5	35	46	<0.0001	0.2		0.007	0.004	0.001	Responsive

The GEMM tumours were refractory to cisplatin, paclitaxel and PLD as the time to PD was the same as for vehicle treated mice. PLD and cisplatin failed to produce any meaningful response with no significant difference in median TTH compared to vehicle treatment. Paclitaxel resulted in modest responses with an increase in median TTH from 15 to 36 days compared to vehicle treated mice ($p = 0.01$). Improvements in time to PD were seen in tumours treated with vinorelbine (56 days) and eribulin (35 days). This led to a significant improvement of median TTH from 15 days for vehicle treated mice to 81 days with vinorelbine ($p < 0.0001$) and to 46 days with eribulin ($p < 0.0001$). The log-rank test was used for statistical analysis of Kaplan-Meier survival curves (Figure 2a). PLD, pegylated liposomal doxorubicin; PD, progressive disease; TTH, time-to-harvest.

Table 2*: In vivo* responses of OCS PDXs to cisplatin, paclitaxel, vinorelbine and eribulin

PDX model	Treatment	Number of mice (n)	Time to PD (days)	Median TTH (days)	p value Compared to vehicle	p value Compared to cisplatin	p value Compared to eribulin	p value Compared to paclitaxel	p value Compared to vinorelbine	Drug response score (Topp et al)
#1040	Vehicle	8	7	53						
	Cisplatin	8	60	120	0.0008					Resistant
	Eribulin	7	>120	>120	0.002	0.1		>1	>1	Sensitive
	Paclitaxel	7	>120	>120	0.001	0.1	>1		>1	Sensitive
	Vinorelbine	6	>120	>120	0.003	0.1	>0.1	>1		Sensitive
PH419	Vehicle	23	7	15						
	Cisplatin	13	7	39	<0.0001					Refractory
	Eribulin	8	>120	>120	<0.0001	0.002		0.09	0.04	Sensitive
	Paclitaxel	14	112	120	<0.0001	0.004	0.09		0.6	Sensitive
	Vinorelbine	12	80	99	<0.0001	0.02	0.04	0.6		Resistant
PH142	Vehicle	31	7	15						
	Cisplatin	19	42	71	<0.0001					Resistant
	Eribulin	10	77	99	<0.0001	0.004		0.8	0.4	Resistant
	Paclitaxel	22	57	95	<0.0001	<0.0001	0.8		0.1	Resistant
	Vinorelbine	19	120	106	<0.0001	<0.0001	0.4	0.1		Sensitive

PH006	Vehicle	17	7	22						
	Cisplatin	9	7	39	0.006					Refractory
	Eribulin	6	>120	>120	0.0005	0.008		0.5	>1	Sensitive
	Paclitaxel	7	>120	>120	<0.0001	0.002	0.5		0.3	Sensitive
	Vinorelbine	7	>120	>120	<0.0001	0.001	>1	0.3		Sensitive
PH003	Vehicle	23	7	8						
	Cisplatin	19	7	15	0.0005					Refractory
	Eribulin	14	7	25	0.0003	0.004		1	0.1	Refractory
	Paclitaxel	16	7	29	<0.0001	0.003	1		0.07	Refractory
	Vinorelbine	13	18	32	<0.0001	0.0005	0.1	0.07		Refractory
PH592	Vehicle	18	7	15						
	Cisplatin	7	7	15	0.03					Refractory
	Eribulin	8	80	92	<0.0001	<0.0001		0.3	0.3	Resistant
	Paclitaxel	8	88	102	<0.0001	<0.0001	0.3		0.2	Resistant
	Vinorelbine	9	63	71	<0.0001	<0.0001	0.3	0.2		Resistant

Cisplatin failed to achieve any meaningful tumour response in four of six PDX models; PH419, PH006, PH003 and PH592. PH142 and #1040 demonstrated some response to cisplatin with improvement of median TTH from 15 to 71 days ($p < 0.0001$) and 53 to 120 days ($p = 0.0008$), compared to vehicle treated mice, respectively. However, times to PD were less than 100 days (PH142 at 42 days and #1040 at 60 days), therefore these tumours were classified as resistant to cisplatin. Three of six PDX (#1040, PH419 and PH006) were shown to be sensitive to paclitaxel *in vivo*, two PDX (PH142 and PH592) were resistant and one PDX (PH003) was refractory based on the same *in vivo* drug response score as cisplatin. Three of six OCS PDX (#1040, PH142 and PH006) were sensitive, two PDXs (PH419 and PH592) were resistant and one PDX (PH003) was refractory to vinorelbine treatment. Three of six OCS PDX models (#1040, PH419 and PH006) were sensitive, two PDX (PH412 and PH592) were resistant and one PDX (PH003) was refractory to eribulin treatment. Significant improvements in median TTH compared with cisplatin treated mice were observed for four models (39 to >120 days for PH419 ($p = 0.002$), 71 to 99 days for PH142 ($p = 0.004$), 39 to >120 days for PH006 ($p = 0.008$), 15 to 25 days for PH003 ($p = 0.004$), and 15 to 92 days for PH592 ($p < 0.0001$)). The log-rank test was used for statistical analysis of Kaplan-Meier survival curves (Figure 4a). PD, progressive disease; TTH, time-to-harvest.

Figure Legends

Figure 1: Mutational and structural variant landscape of ovarian carcinosarcoma

(A) Summary of frequently altered genes across the carcinoma, sarcoma and metastasis samples from 18 macrodissected ovarian carcinosarcoma samples. For missense mutations, light green represents "unknown significance" and dark green represents "putative driver". Metastases are colour-coded according to their histology. **(B)** Mutation burden (mutations per megabase sequenced). **(C)** Comparison of EMT scores in separated carcinomatous and sarcomatous regions from ovarian carcinosarcoma samples, whole ovarian carcinosarcoma tumours, and ovarian high-grade serous carcinoma samples in TCGA. **(D)** Expression of *MYCN*, *LIN28B* and *HMGA2* in our ovarian carcinosarcoma cohort compared to ovarian high-grade serous carcinoma tumours in TCGA. Data were analysed using the non-parametric Wilcoxon rank-sum test. TCGA-OV, ovarian high-grade serous carcinomas in TCGA; C, carcinoma; S, sarcoma; M, metastasis.

Figure 2: GEMM OCS tumours were refractory to current standard-of-care treatments for ovarian cancer but were responsive to the microtubule drugs vinorelbine and eribulin

(A) *In vivo* treatment of GEMM OCS tumours with: DPBS (n=25), cisplatin (4mg/kg; n=10), PLD (1.5mg/kg; n=3), paclitaxel (25mg/kg; n=3), vinorelbine (15mg/kg; n=9) and eribulin (1.5mg/kg; n=5). Dashed lines denote end of treatment period. Shaded area = 95% confidence interval. Time to PD and harvest (TTH) are shown in Table 1. **(B)** Representative images of Ki67 assessed by IHC in a number of tumours after a single dose of eribulin (or DPBS vehicle). Scale bars represent 100 μm. The percentage of Ki67 cells was quantified in 6 fields of view per tumour; ***p<0.001. **(C)** GEMM cells were pre-treated with IC_{20} concentrations of eribulin (20 nM) or cisplatin (0.2 μM), or vehicle control (DMSO) for one week before being plated in adhesion assays (left panel) or migration and invasion assays (right panel). Percentage of adherent cells was calculated compared to vehicle-treated controls. Percentage of invading cells was calculated compared to number of migrating cells. Bar graphs represent the mean and standard error across independent experimental repeats (n=3-5); *p<0.05, **p<0.01. **(D)** GEMM cells were pre-treated as above with eribulin, cisplatin or vehicle control (DMSO) for one week before being plated in collagen with treatment either removed or maintained. Representative images of colonies growing in collagen on day 8 are shown. Scale bars represent 200 μm. **(E)** Expression of the mesenchymal markers ZEB1, N-cadherin, vimentin and HMGA2 in cells exposed to an IC_{50} concentration of eribulin (50 nM) or DMSO control for the indicated time-points was determined by Western Blot analysis. β-actin was used as a

loading control. PLD, pegylated liposomal doxorubicin; PD, progressive disease; IHC, immunohistochemistry.

Figure 3: Characterisation of PDX models of OCS with varying proportions of carcinoma and sarcoma

(A) Tumours from each PDX model of OCS were assessed by IHC. Representative images of H&E, Ki67, p53, PAX8, pan-CK, vimentin and HMGA2 staining are shown. Scale bars represent 100 μm. Proportions of carcinoma and sarcoma in each model, as assessed by a gynaecological pathologist, are indicated below the images. #1040 and PH419 were almost purely carcinoma, PH142, PH006 and PH003 were mixed with both carcinomatous and sarcomatous characteristics (i.e. expressing both pan-CK and vimentin) and PH592 was purely sarcomatous, with some epithelial characteristics (i.e. pan-CK co-expression in some cells). **(B)** Expression of *HMGA2*, *LIN28B* and *MYCN* were determined from RNAseq data for each OCS model (n=3) compared to ovarian high-grade serous carcinoma samples in TCGA (n=379). **(C)** EMT scores generated from RNAseq data for tumours from each OCS PDX model are shown compared with EMT scores for ovarian high-grade serous carcinoma samples in TCGA. **(D)** Expression of the mesenchymal markers ZEB1, N-cadherin, vimentin and HMGA2 in tumours from each OCS PDX model was determined by Western Blot analysis. β-actin was used as a loading control. PDX, patient-derived xenograft; IHC, immunohistochemistry; CK, cytokeratin; TCGA-OV, ovarian high-grade serous carcinomas in TCGA; CLR, centred log ratio; EMT, epithelial-to-mesenchymal transition; PH003m, PH003mixed; PH003s, PH003sarc.

Figure 4: PDX OCS tumours were refractory to cisplatin but displayed mostly impressive responses to microtubule drugs

(A) *In vivo* treatment of OCS PDX tumours with DPBS, cisplatin (4mg/kg), paclitaxel (25mg/kg), vinorelbine (15mg/kg) and eribulin (1.5mg/kg, with the exception of mice harbouring #1040 tumours, which received doses of 1mg/kg). n values for each model are shown in Table 2. Dashed lines denote end of treatment period. Shaded area = 95% confidence interval. More carcinomatous models are shown on the top left and the more sarcomatous models on the bottom right. Time to PD and harvest (TTH) are shown in Table 2. **(B)** Expression of HMGA2 in tumours from each OCS PDX model after a single dose of vehicle (DPBS) or eribulin was determined by IHC. Scale bars represent 100 μm. **(C)** Expression of the mesenchymal markers ZEB1 and N-cadherin in tumours from each OCS PDX model after

a single dose of vehicle (DPBS) or eribulin was determined by Western Blot analysis. β-actin was used as a loading control. **(D)** Quantification of expression data in (C). *p<0.05, **p<0.01.

Figure 5: The mevalonate pathway was down-regulated following eribulin treatment of OCS cells and tumours as a result of increased cellular cholesterol

(A) Analysis of GO terms enriched for down-regulated (left) and up-regulated (right) DEGs. Circle sizes indicate DEGs present in each GO term. DEGs are listed in Supplementary Tables S20 - S23. **(B)** Expression of N-MYC, HMGCS, SQLE and LDLR in tumours from each OCS PDX model after a single dose of vehicle (DPBS) or eribulin was determined by Western Blot analysis. β-actin was used as a loading control. **(C)** Quantification of expression data in (B). **(D)** Quantification of total cholesterol, free cholesterol and cholesterol ester in tumours from each OCS PDX model after a single dose of vehicle (DPBS) or eribulin. **(E)** Representative images of Oil Red O staining in PH419 tumours following a single dose of vehicle (DPBS) or eribulin. Scale bar = 100 μm. **(F)** Expression of the mesenchymal markers ZEB1 and N-cadherin, as well as the MVA pathway proteins HMGCS, SQLE and LDLR, in PH419 cells exposed to 15nM of eribulin or DMSO control for the indicated time-points, was determined by Western Blot analysis. β-actin was used as a loading control. **(G)** Quantification of total cholesterol, free cholesterol and cholesterol ester in PH419 cells exposed to 15nM of eribulin or DMSO control for the indicated time-points. Bar graphs represent the mean and standard error across independent experimental repeats (n=3); *p<0.05, **p<0.01 and ***p<0.001. GO, gene ontology; DEG, differentially expressed gene; FDR, false discovery rate; MVA, mevalonate pathway; TC, total cholesterol; FC, free cholesterol; CE, cholesterol ester.

Figure 6: PDX tumours have a greater percentage of human CD8-positive T-cells following eribulin treatment. (A) Blood from NSG mice reconstituted with human CD34+ haematoietic stem cells was analysed 12 weeks post-reconstitution by flow cytometry to determine proportion of human immune cells present. **(B)** PDX tumours harvested one week after mice received a single dose of vehicle (DPBS), eribulin (3mg/kg) or cisplatin (4mg/kg) were analysed by IHC. Representative images of tumour infiltrating CD8-positive T-cells are shown for each model and treatment. Scalebar = 50μm. **(C)** Percentage of CD8-positive T-cells was quantified in 20 fields of view at 400x magnification for each tumour and is shown for individual mice. Statistical analysis was performed using the Kruskal-Wallis test. **p<0.01, ****p<0.0001.

Figure 1

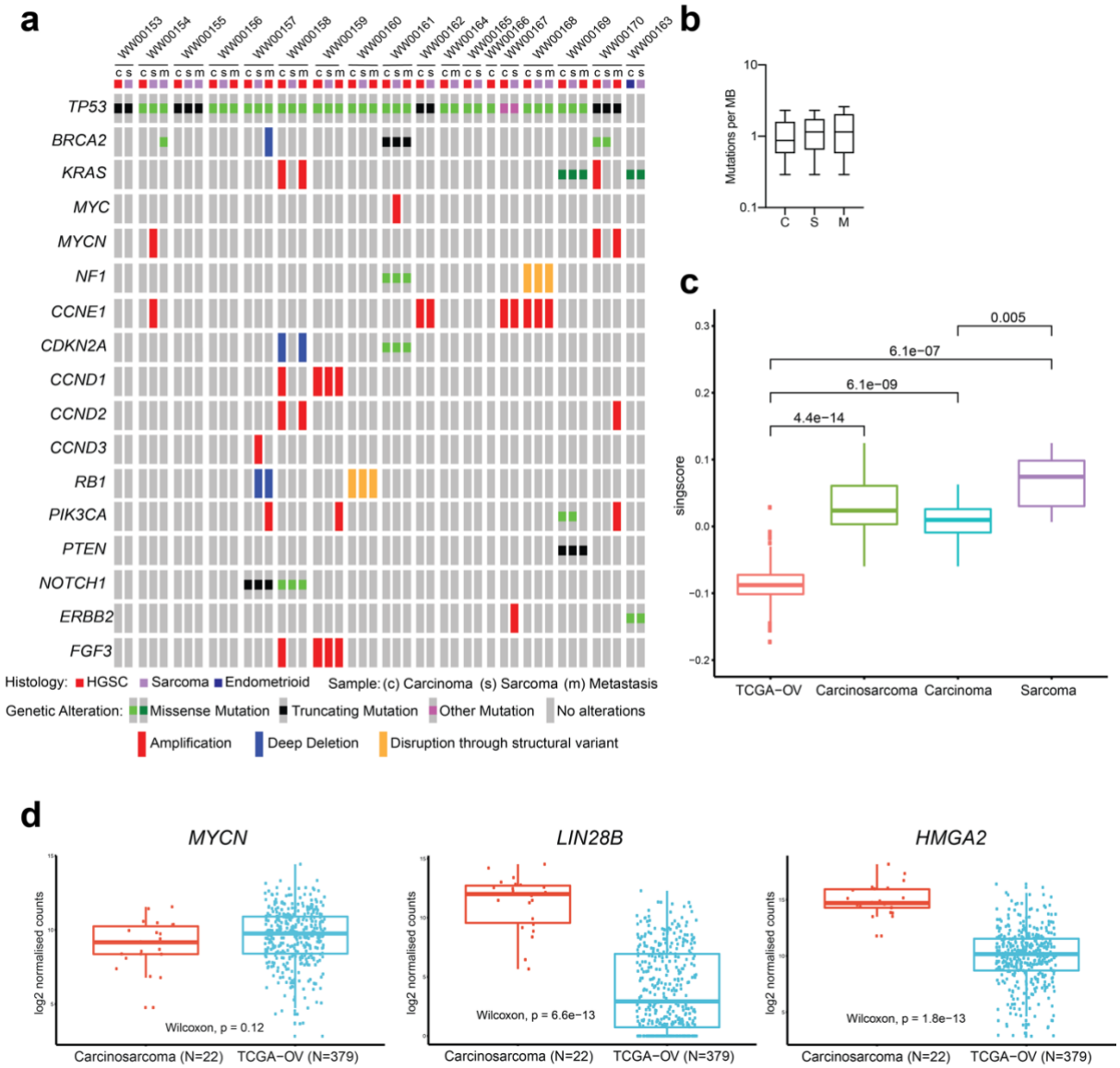
a
b
c
d
TP53
BRCA2
KRAS
MYC
MYCN
NF1
CCNE1
CDKN2A
CCND1
CCND2
CCND3
RB1
PIK3CA
PTEN
NOTCH1
ERBB2
FGF3
Histology: HGSC Sarcoma Endometrioid
Sample: (c) Carcinoma (s) Sarcoma (m) Metastasis
Genetic Alteration: Missense Mutation Truncating Mutation Other Mutation No alterations
Amplification Deep Deletion Disruption through structural variant
Mutations per MB
singscore
0.005
6.1e−07
6.1e−09
4.4e−14
TCGA−OV
Carcinosarcoma
Carcinoma
Sarcoma
MYCN
LIN28B
HMGA2
log2 normalised counts
Wilcoxon, p = 0.12
Wilcoxon, p = 6.6e−13
Wilcoxon, p = 1.8e−13
Carcinosarcoma (N=22)
TCGA−OV (N=379)

Figure 2

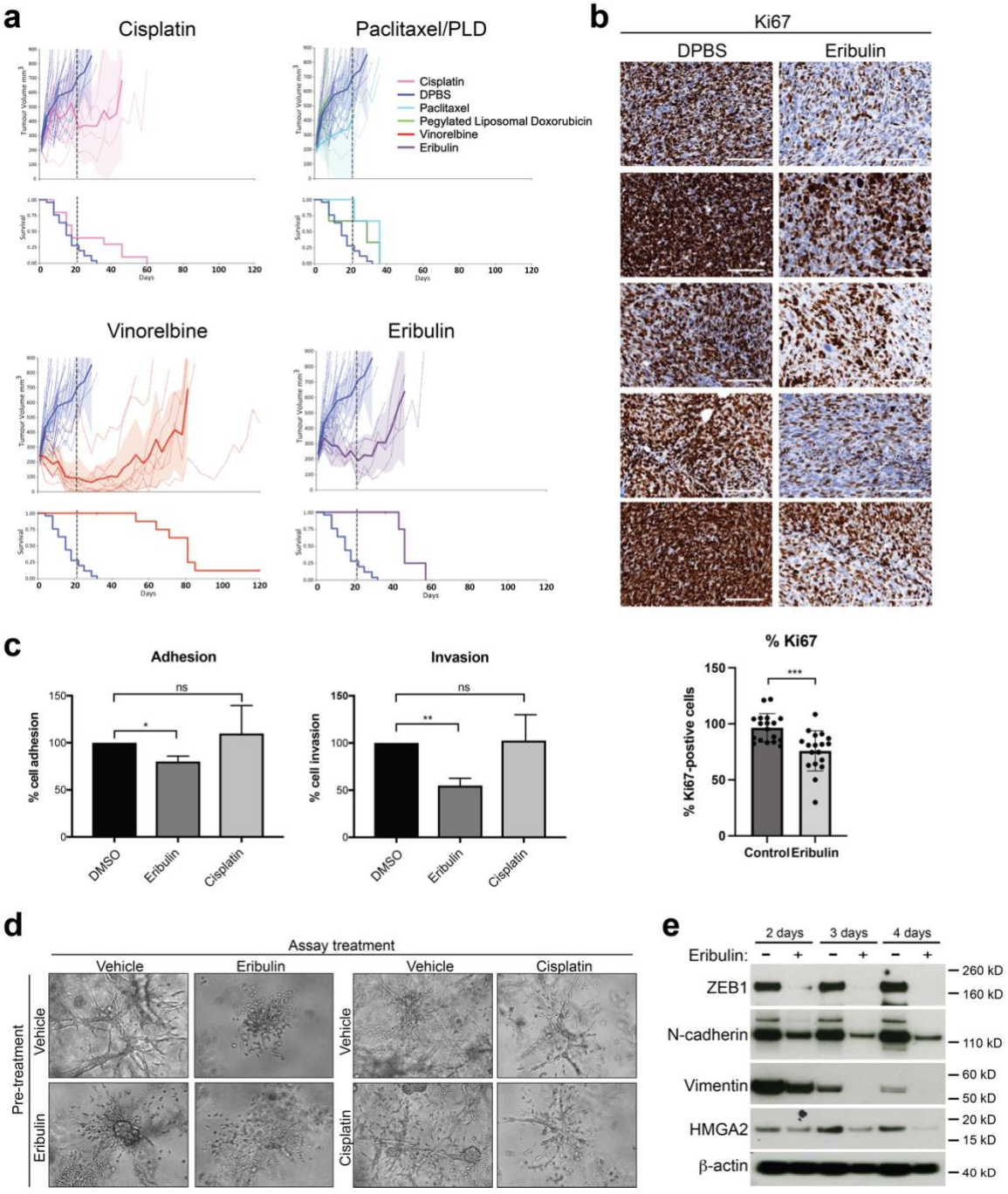

1127

Figure 3

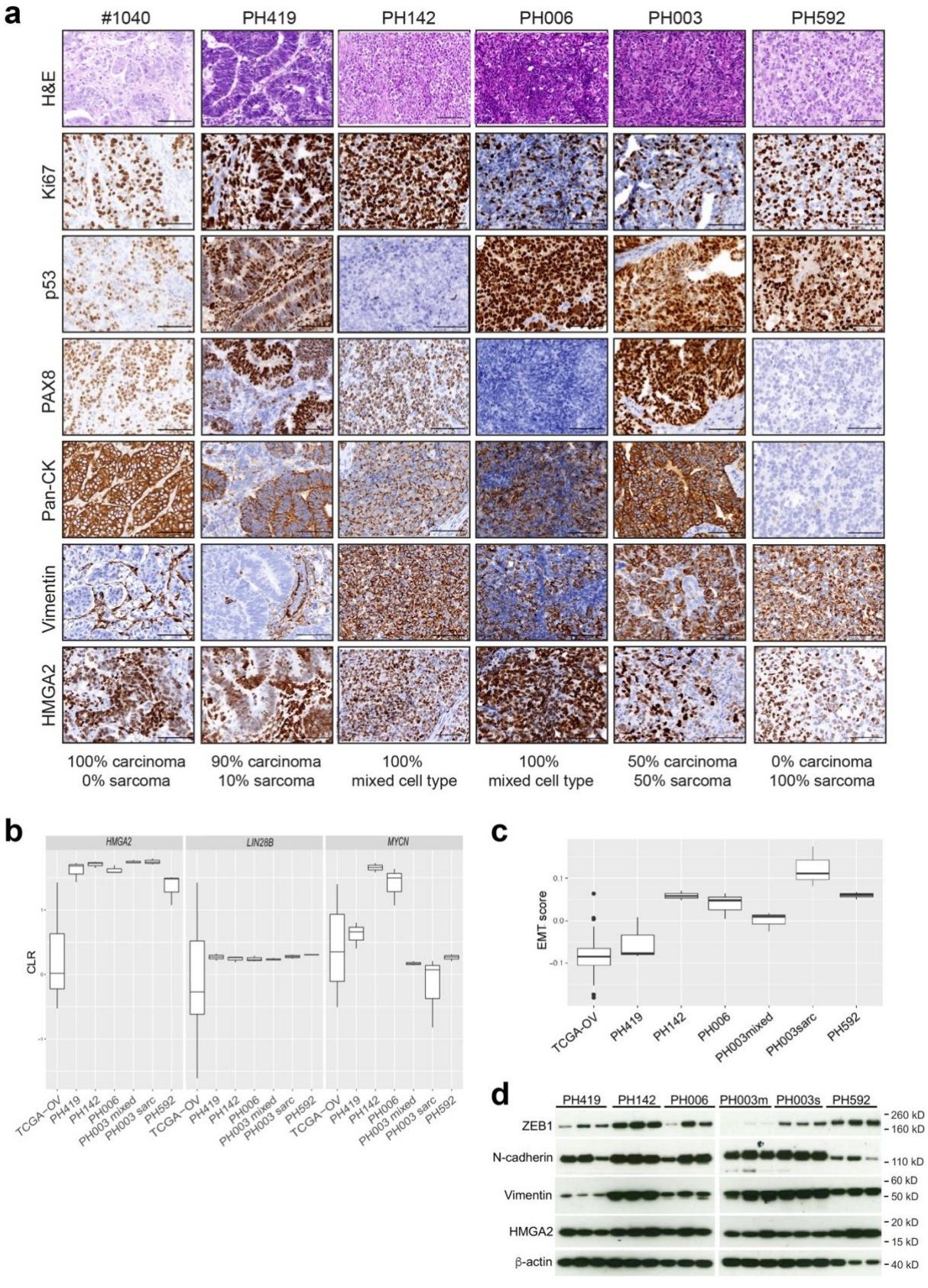
a
#1040
PH419
PH142
PH006
PH003
PH592
H&E
Ki67
p53
PAX8
Pan-CK
Vimentin
HMGA2
100% carcinoma
0% sarcoma
90% carcinoma
10% sarcoma
100%
mixed cell type
100%
mixed cell type
50% carcinoma
50% sarcoma
0% carcinoma
100% sarcoma
b
HMGA2
LIN28B
MYCN
CLR
TCGA-OV
PH419
PH142
PH006
PH003 mixed
PH003 sarc
PH592
c
EMT score
TCGA-OV
PH419
PH142
PH006
PH003mixed
PH003sarc
PH592
d
PH419
PH142
PH006
PH003m
PH003s
PH592
ZEB1
N-cadherin
Vimentin
HMGA2
β-actin
260 kD
160 kD
110 kD
60 kD
50 kD
20 kD
15 kD
40 kD

Figure 4

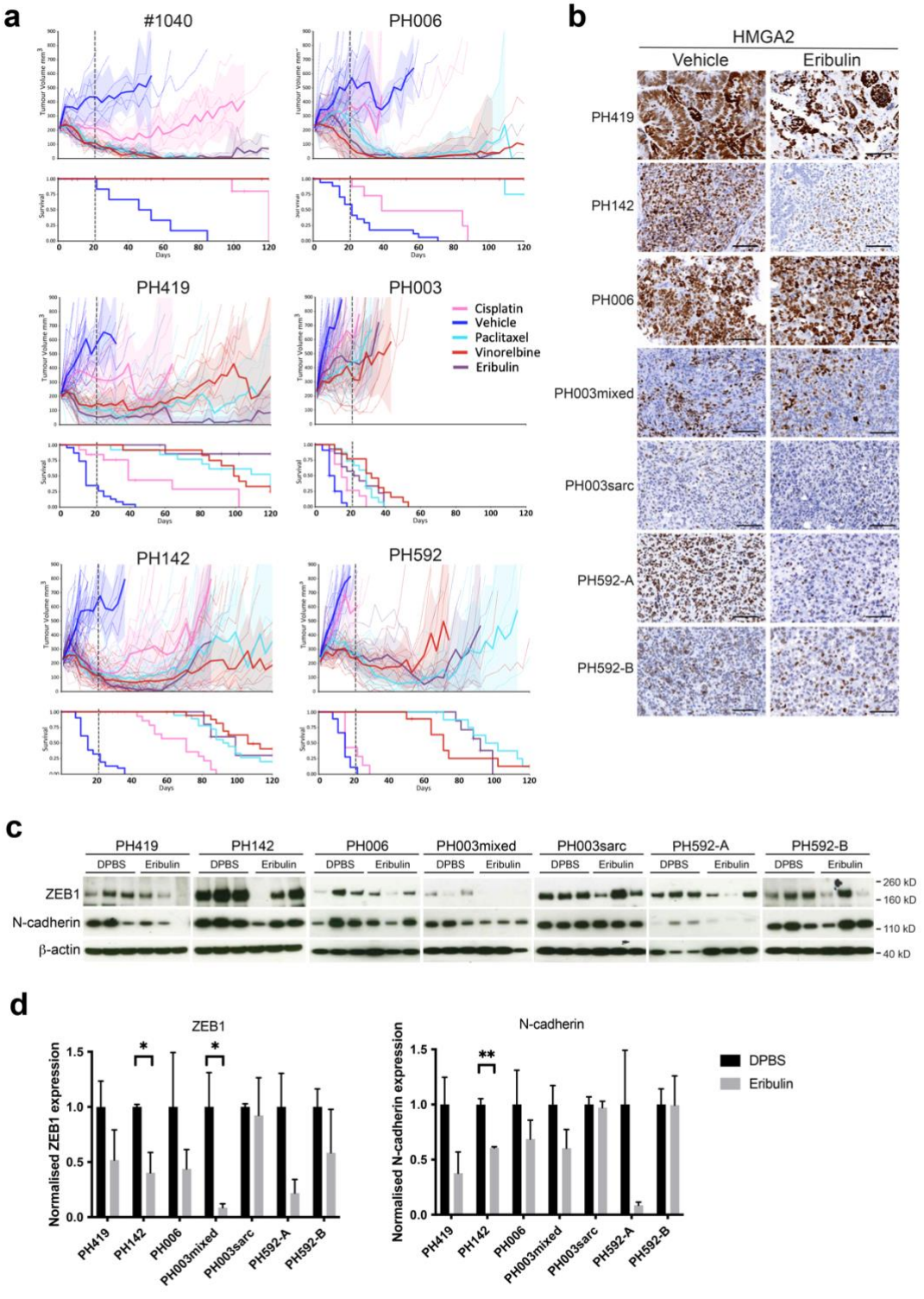
a
#1040
PH006
PH419
PH003
PH142
PH592
Cisplatin
Vehicle
Paclitaxel
Vinorelbine
Eribulin
Tumour Volume mm3
Survival
Days
b
HMGA2
Vehicle
Eribulin
PH419
PH142
PH006
PH003mixed
PH003sarc
PH592-A
PH592-B
c
PH419
PH142
PH006
PH003mixed
PH003sarc
PH592-A
PH592-B
DPBS
Eribulin
ZEB1
N-cadherin
β-actin
260 kD
160 kD
110 kD
40 kD
d
ZEB1
N-cadherin
Normalised ZEB1 expression
Normalised N-cadherin expression
DPBS
Eribulin
PH419
PH142
PH006
PH003mixed
PH003sarc
PH592-A
PH592-B

Figure 5

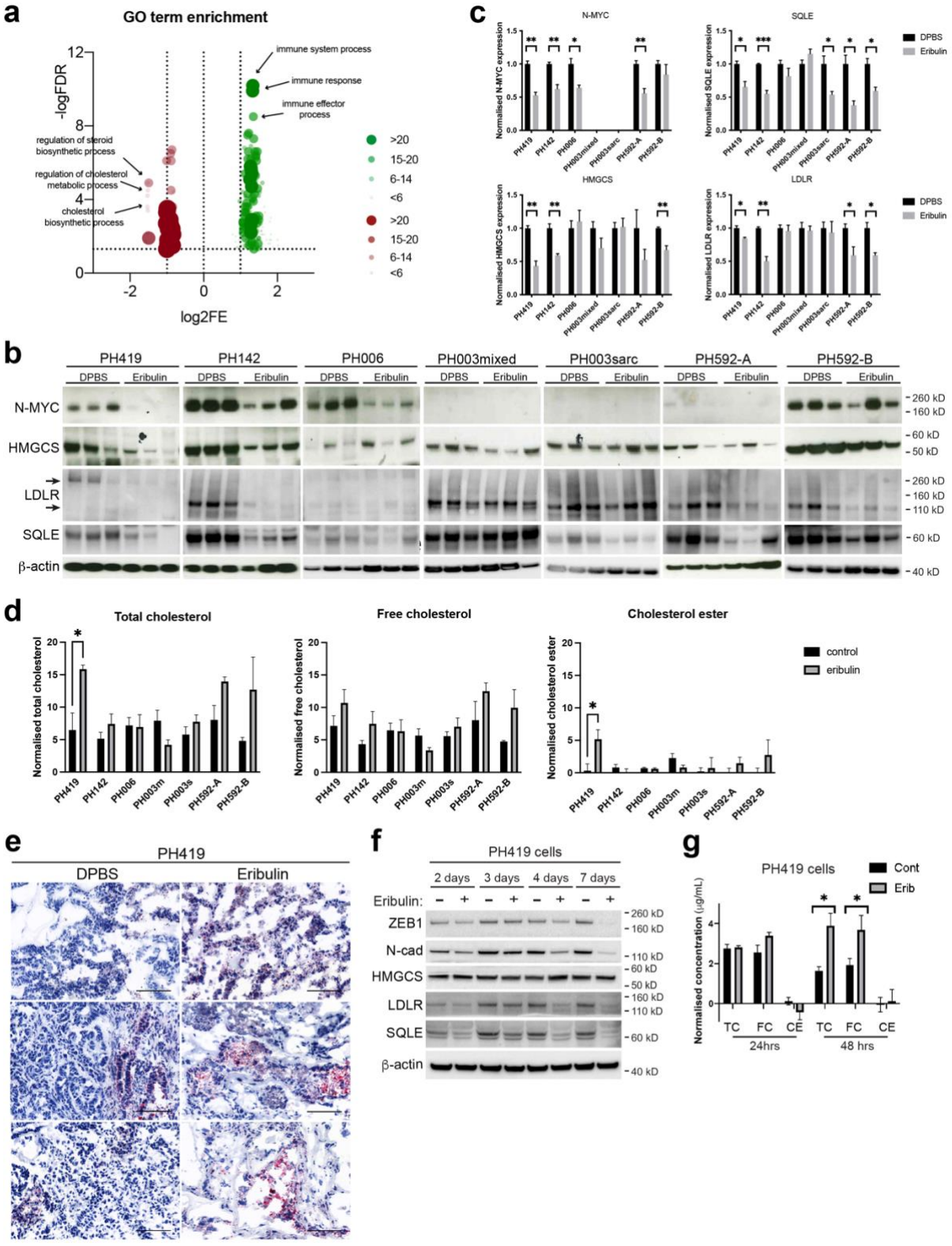

1132

Figure 6

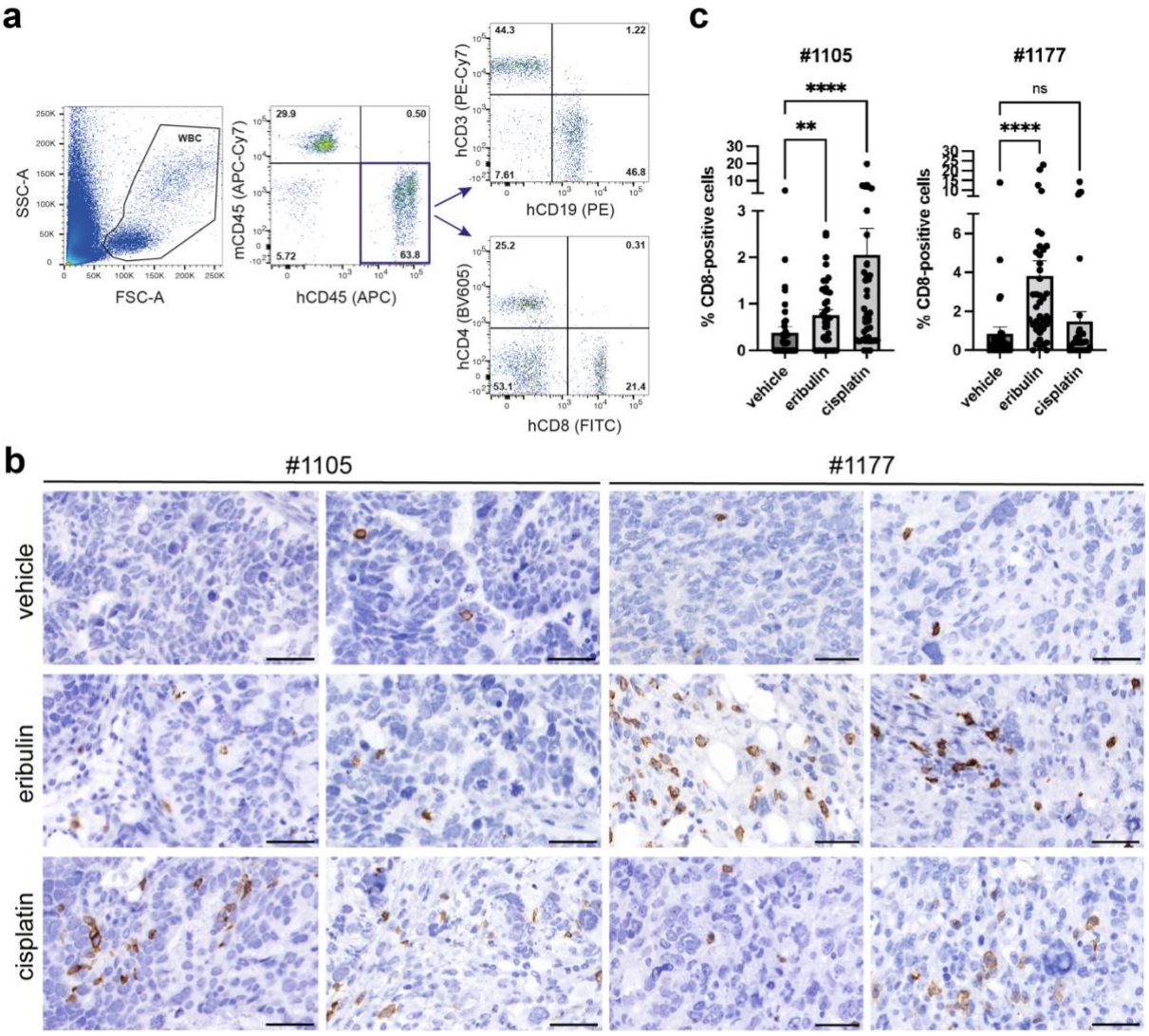

1133